technology) and developed with horseradish peroxidase-coupled secondary antibodies, followed by enhancement with a chemiluminescence (ECL) detection system (GE Healthcare).

Generation of Adenoviruses—Adenoviruses carrying GFP or Cry1 were constructed using the ViraPower Adenoviral Expression System (Invitrogen). Briefly, cDNA was inserted into a TOPO pENTR vector and was recombined to the adenovirus expression plasmid pAd/CMV/V5-DEST. The pAd/CMV/V5-DEST plasmid with the cDNA of interest was digested with the PacI endonuclease and transfected with HEK293A cells. The medium supernatant containing the adenovirus was collected and titrated according to the manufacturer's instructions. UMR-106 cells were infected with the adenovirus at a multiplicity of infection of 500 with 4 μg/ml poly-L-lysine (Sigma).

Constructs and Luciferase Reporter Assay—The Cry1 expression construct with a V5 tag was created by subcloning the corresponding PCR products into the pENTR vector using the pENTR Directional TOPO cloning kit (Invitrogen) and transferring to the pcDNA3.2/V5 vectors using the LR recombination reaction system (Invitrogen). Luciferase vectors containing 2000 bp of the mouse *Fgf23* gene promoter (−1872 to +128) (2000bp-Luc) was prepared by subcloning the corresponding PCR products into pGL4.20[luc2/Puro] (Promega, Madison, WI) vectors according to the previous report (13). Luciferase constructs containing 766 bp (−638 to +128) of the *Fgf23* gene promoter were created by the digestion of 2000bp-Luc with BglII (located at the 5′ region in the multiple cloning site of the pGL4.20 vector relative to the insert and −638 to −633) followed by the ligation of fragments containing luciferase with T4 DNA ligase. Luciferase constructs containing 143 bp (−15 to +128) of the *Fgf23* gene promoter were designed by digesting pT7 vectors harboring 2000 bp of the *Fgf23* gene promoter with SmaI (located at −18 to −13 and the 3′ region in the pT7 vector relative to the insert) followed by the ligation of fragments containing the promoter region of interest with pGL4.20[luc2/Puro] vectors digested with EcoRV using T4 DNA ligase.

Mutagenesis—Two candidate motifs were detected as possible cAMP responsive elements (CREs) in the promoter region of the *Fgf23* gene by *in silico* analysis, and these motifs were designated as CRE1 and CRE2, respectively. To determine whether these motifs were functional, site-directed mutagenesis was performed using QuikChange II XL (Agilent Technologies, Santa Clara, CA) according to the manufacturer's protocol. The CRE1 located at −620 to −613 and CRE2 located at −46 to −39 were mutated from TGACCTCA to TGAAATCA and TGATGTCA to TGAAATCA, respectively.

Luciferase Assay—UMR-106 cells were seeded in a 24-well plate at a density of 5×10^4 cells/well, and transient transfection was carried out using FuGENE HD (Promega) following the manufacturer's protocol. The total amount of DNA added to each well was equalized using an empty vector. The luciferase assay was performed in triplicate according to the protocol of the dual-luciferase reporter assay system (Promega). Briefly, 24 h after transfection cells were treated with isoproterenol (10 or 100 μM) and/or IBMX (0.5 mM) in DMEM containing 1% FCS overnight, followed by the determination of luciferase activity using specific substrates in a luminometer. Transfection efficiency was normalized by co-transfection with the TK-*Renilla* luciferase construct (Promega). While Cry1-overexpressing UMR-106 cells were used for the luciferase assay, UMR-106 cells were infected with an adenovirus containing GFP or Cry1-V5. Twenty-four h after the infection cells were trypsinized and plated in a 24-well plate as described above.

Animal Studies—Isoproterenol or PTH(1–34) was dissolved in saline and administered intraperitoneally at a dose of 6 μg/g (32) or 100 μg/kg, respectively. A saline injection was used as a control treatment. Whereas propranolol (PRO) was used for the *in vivo* study, PRO was dissolved in the drinking water at a concentration of 0.5 g/liter (33), and the drinking water was changed three times a week.

Measurement of Serum and Urine Parameters—The measurement of serum phosphate was carried out using P-test Wako (Wako Pure Chemical Industries Ltd., Osaka, Japan). Total (C-Term) and intact (full-length) FGF23 concentrations were determined by ELISA from Immutopics, Inc., San Clemente, CA and Kainos Laboratory, Tokyo, Japan, respectively, following the manufacturers' instructions. Urine samples were collected in the presence of 5 μl of 5 N HCl, and the volume of urine was measured. Urine epinephrine was determined using ELISA (IBL, Hamburg, Germany). Urine phosphate and creatinine were measured using P-test Wako and Creatinine Test Kit (Wako Pure Chemical Industries Ltd.), respectively.

Statistical Analysis—All data are expressed as the mean ± S.E. Results were examined for significant differences using Student's *t* test or analysis of variance followed by the Bonferroni multiple comparison *post hoc* test. Significance was set at $p < 0.05$.

RESULTS

Skeletal Fgf23 Exhibited a Circadian Expression Profile—To investigate the mechanisms whereby phosphate metabolism is regulated by the circadian clock network, we first examined the circadian expression profile of *Fgf23* in the femur of wild-type mice fed standard chow *ad libitum* (AL). As reported previously (34), components of the clock network including *Rev-erbα* (nuclear receptor subfamily 1, group D, member 1; Nr1d1), *Dbp* (D site of albumin-binding protein), and *Cry1* exhibited rhythmic expression patterns in the femur (Fig. 1, *A–C*, and supplemental Fig. S1). The *Fgf23* expression profile showed higher expression levels during the dark phase (DP) compared with the light phase (LP) with the highest at ZT16 (Fig. 1*D* and supplemental Fig. S1). Because it is well known that food consumption reaches highest at the beginning of DP in mice fed AL, we speculated that skeletal *Fgf23* expression was regulated by the food consumption in a manner involving the circadian clock system. To test this speculation, mice were fed during the LP from ZT2 to ZT8 (LP-restricted feeding: LP-RF) for 10 days. Because it is unclear whether skeletal tissue is entrained by nutrient availability despite the fact that food intake is a strong zeitgeber in peripheral tissues such as liver, we examined the circadian expression profiles of genes involved in daily oscillations in the femur. As shown in Fig. 2, *A–C*, and supplemental Fig. S2, the peak expressions of *Rev-erbα*, *Dbp*, and *Cry1* shifted by 12 h in mice under LP-RF conditions compared with AL conditions, suggesting that skeletal tissue is also

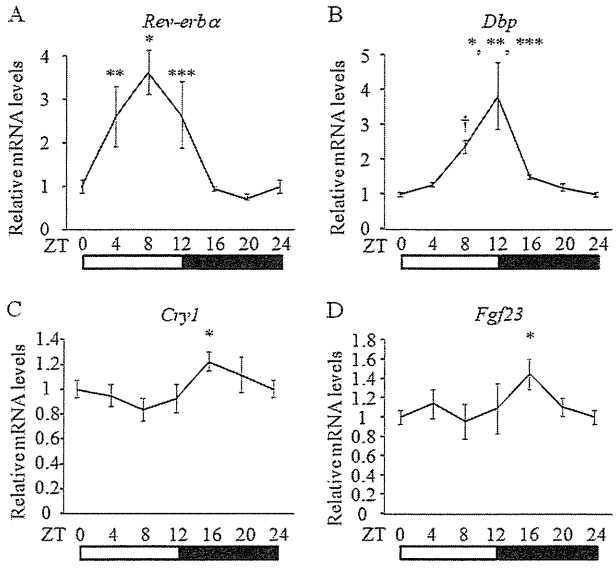

FIGURE 1. **Fgf23 showed a rhythmic expression pattern in the femur of mice fed *ad libitum*.** WT mice were maintained under a light-dark regimen (12-h:12-h cycle) and fed *ad libitum*. Samples were collected every 4 h from ZT0. *A*, expression of *Rev-erbα* ($n = 3–4$, *, $p < 0.01$ *versus* ZT0 and ZT20; **, $p < 0.05$ *versus* ZT20; ***, $p < 0.05$ *versus* ZT0, ZT16 and ZT20). *B*, expression of *Dbp* ($n = 3$, *, $p < 0.001$ *versus* ZT0, ZT4, and ZT20; **, $p < 0.01$ *versus* ZT16; ***, $p < 0.05$ *versus* ZT8; †, $p < 0.05$ *versus* ZT0). *C*, expression of *Cry1* ($n = 5–7$, *, $p < 0.05$ *versus* ZT8). *D*, expression of *Fgf23* ($n = 5–7$, *, $p < 0.05$ *versus* ZT8). All expression was in the femur and was analyzed using real-time RT-PCR. The *white bar* and *black bar* represent the light phase and dark phase, respectively. Values are expressed as the mean ± S.E. (*error bars*).

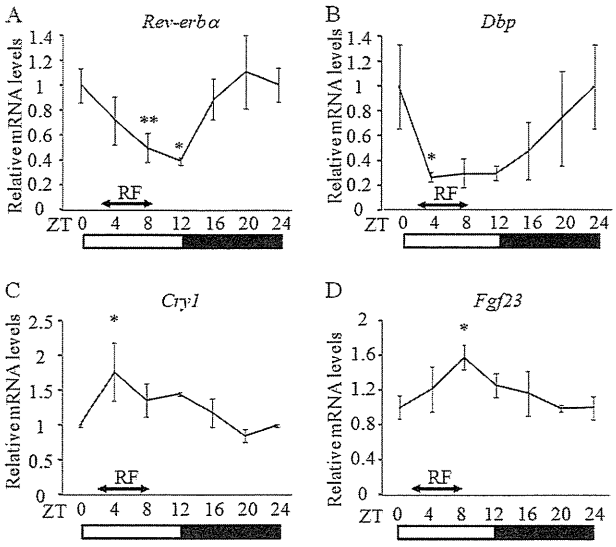

FIGURE 2. **Light phase restricted feeding altered the expression profile of *Fgf23* in the femur.** WT mice were maintained under a light-dark regimen (12-h:12-h cycle) and fed for 6 h from ZT2 to ZT8 for 10 days. Samples were collected every 4 h from ZT0. *A*, expression of *Rev-erbα* ($n = 3$, *, $p < 0.05$ *versus* ZT0 and ZT20; **, $p < 0.05$ *versus* ZT20). *B*, expression of *Dbp* ($n = 3$, *, $p < 0.05$ *versus* ZT0). *C*, expression of *Cry1* ($n = 3–4$, *, $p < 0.05$ *versus* ZT0 and ZT20). *D*, expression of *Fgf23* ($n = 3$, *, $p < 0.05$ *versus* ZT0). All expression was in the femur and was determined by real-time RT-PCR. The *white bar* and *black bar* represent the light phase and dark phase, respectively. Values are expressed as the mean ± S.E. (*error bars*).

entrained by nutrient availability. Based on this observation, we next analyzed the expression profile of *Fgf23* in the femur and found that *Fgf23* showed a rhythmic expression pattern with a peak expression at ZT8 (Fig. 2*D* and supplemental Fig. S2). Taken together, these findings indicate that *Fgf23* expression

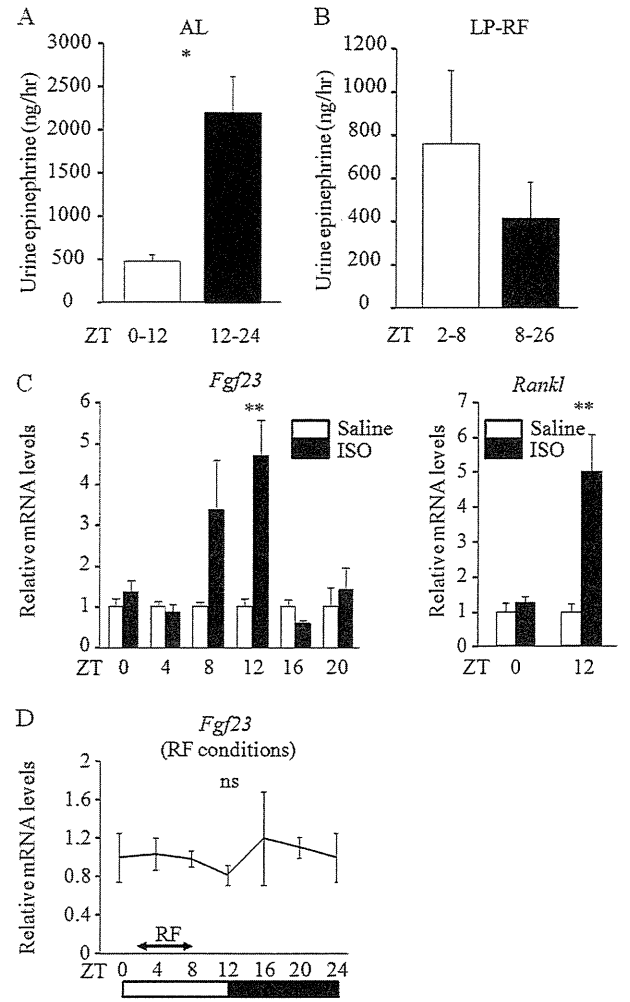

FIGURE 3. **Sympathetic activation induced skeletal *Fgf23* expression *in vivo*.** *A*, urine was collected from WT mice under *ad libitum* (*AL*) conditions either during the light phase (LP: ZT0–12) or the dark phase (ZT12–24). The volume of urine and urine epinephrine levels were measured, and the amount of urine epinephrine/h was determined ($n = 9$). *B*, urine was collected from WT mice under LP-RF conditions either during ZT2–8 or ZT8–26. The volume of urine and urine epinephrine levels were measured, and the amount of urine epinephrine/h was determined ($n = 7$). *C*, ISO was administered intraperitoneally to WT mice under AL conditions at different time points of the day as indicated, and 4 h after the injection the expression of *Fgf23* and *Rankl* in the femur was determined by real-time RT-PCR ($n = 3–4$). *D*, WT mice were maintained under LP-RF conditions for 10 days, and 0.5 g/liter propranolol was added to the drinking water from day 7 to day 10. Femurs were collected at indicated time points, and *Fgf23* expression was measured by real-time RT-PCR ($n = 3$). The *white bar* and *black bar* represent the light phase and dark phase, respectively. *ns*, not significantly different. Values are expressed as the mean ± S.E. (*error bars*). *, $p < 0.001$; **, $p < 0.05$.

possesses a circadian expression profile that is at least in part determined by the time of nutrient availability.

Sympathetic Activation Enhanced Fgf23 Expression in the Femur—It is well known that food intake is tightly coupled to an increase in the metabolic rate to adjust for the increase in nutrient influx, which in part involves an elevation in sympathetic activity (25–28). Indeed, urine levels of epinephrine, a marker for sympathetic activity, in mice fed AL were significantly enhanced in DP compared with LP (Fig. 3*A*). Interestingly, LP-RF caused a phase shift in sympathetic activity with greater levels during LP-RF, but the difference did not reach statistical significance (Fig. 3*B*). Based on these findings, we speculated

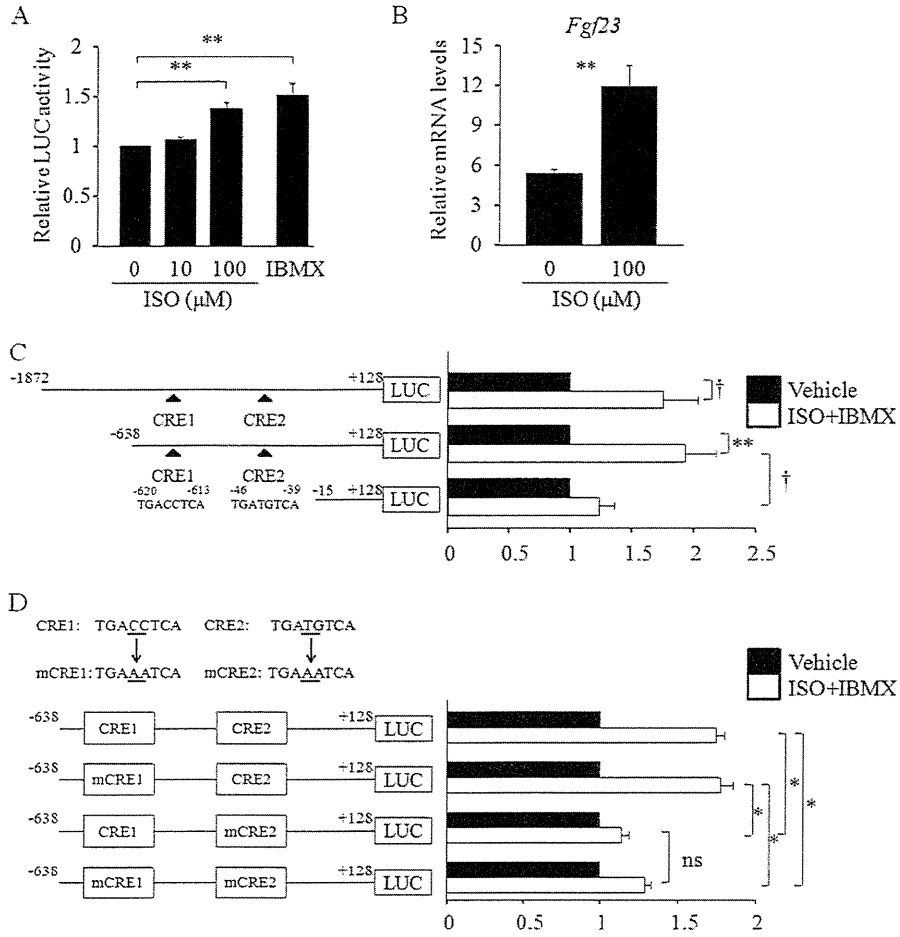

FIGURE 4. **ISO trans-activated *Fgf23* transcription in UMR-106 cells.** *A*, UMR-106 cells were seeded in 24-well plates and transfected with 2000bp-Luc (200 ng) and phRL-TK (10 ng). Twenty-four h after transfection, cells were treated with ISO at a dose of 10 or 100 μM overnight, and luciferase activity was measured. 0.5 mM IBMX was used as a positive control for the activation of cAMP signaling ($n = 3$). *B*, UMR-106 cells were treated with 100 μM ISO overnight, and expression of *Fgf23* was determined by real-time RT-PCR ($n = 4$). *C*, UMR-106 cells were seeded in 24-well plates and transfected with 2000bp-Luc (200 ng), 766bp-Luc (200 ng), or 143bp-Luc (200 ng) and phRL-TK (10 ng). Twenty-four h after transfection, cells were treated with ISO (100 μM) and IBMX (0.5 mM) overnight, and luciferase activity was measured ($n = 5$). *D*, UMR-106 cells were seeded in 24-well plates and transfected with 766bp-Luc (200 ng) or 766bp-Luc containing mutations in CRE1 and/or CRE2 (200 ng), and phRL-TK (10 ng). Twenty-four h after transfection, cells were treated with ISO (100 μM) and IBMX (0.5 mM) overnight, and luciferase activity was measured ($n = 4$). Values are expressed as the mean ± S.E. (*error bars*). *ns*, not significantly different. *, $p < 0.001$; **, $p < 0.01$; †, $p < 0.05$.

that *Fgf23* expression may at least in part be regulated by sympathetic activation in a circadian manner. To test this idea, we intraperitoneally administered the β-adrenergic receptor agonist, isoproterenol (ISO), to mice at different time points of the day and analyzed the expression of *Fgf23* in the femur 4 h after the injection. The administration of ISO caused an increase in skeletal *Fgf23* expression when injected at ZT8 ($p = 0.12$) and ZT12 ($p < 0.05$), whereas ISO treatment had no effect on *Fgf23* expression when administered at the other time points (Fig. 3*C*). To determine whether the effect of ISO was specific to *Fgf23* induction, we also analyzed the expression of *Rankl*, one of the target genes of ISO (35), and found that the induction of *Rankl* showed a pattern similar to that of *Fgf23* induction (Fig. 3*C*). To further understand the involvement of sympathetic activity in the circadian *Fgf23* profile, mice were maintained under LP-RF in the presence of the β-blocker, PRO, to analyze the effect of sympathetic activity on the peak expression of *Fgf23* noted at ZT8. Interestingly, *Fgf23* expression did not exhibit any circadian profile when PRO was concomitantly administered, indicating the involvement of sympathetic activity in the circadian profile of *Fgf23* expression in the femur (compare Fig. 3*D* with Fig. 2*D*, and see supplemental Fig. S2).

ISO Trans-activated the Fgf23 Gene Promoter and Induced Fgf23 Expression in UMR-106 Cells—Because *in vivo* administration of ISO enhanced the expression of *Fgf23* in the femur, we investigated whether ISO signaling trans-activated *Fgf23* gene promoter using osteoblastic UMR-106 cells in which endogenous *Fgf23* was expressed. For this purpose, we generated a luciferase construct containing a 2000-bp promoter region of the mouse *Fgf23* gene. The treatment with ISO showed a significant increase in luciferase activity in a dose-dependent manner (Fig. 4*A*). In line with this, the ISO treatment enhanced the expression of *Fgf23* in these cells (Fig. 4*B*). These results suggest that ISO induces *Fgf23* expression at least in part by activating the transcription of the *Fgf23* gene. Because *in silico* analysis pointed out the existence of two motifs whose sequences were very similar to CRE, we next tested whether these motifs, designated as CRE1 and CRE2, respectively, were involved in ISO-induced *Fgf23* trans-activation. For this purpose, we generated luciferase vectors containing the truncated

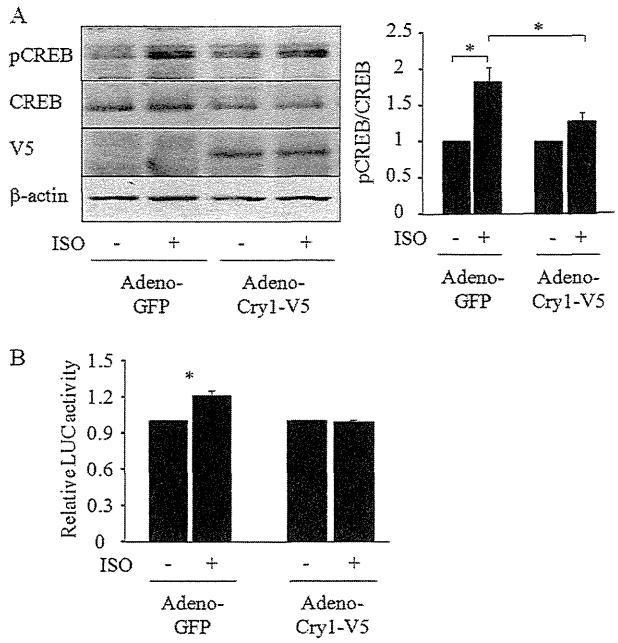

FIGURE 5. **Cry1 suppressed ISO-induced phosphorylation of CREB in UMR-106 cells.** *A*, UMR-106 cells were infected with an adenovirus containing GFP or Cry1-V5 and treated with 100 μM ISO for 5 min. The expression of pCREB, CREB, V5, and β-actin was determined by Western blotting, and expression of pCREB was quantified by normalizing to the levels of CREB by densitometric analysis ($n = 5$). *B*, UMR-106 cells infected with an adenovirus containing either GFP or Cry1 were seeded in 24-well plates and transfected with 2000bp-Luc (200 ng) and phRL-TK (10 ng). Twenty-four h after transfection cells were treated with 100 μM ISO overnight, and luciferase activity was measured ($n = 3$). The figures shown are the representative from at least three independent experiments. Values are expressed as the mean ± S.E. (*error bars*). *, $p < 0.05$.

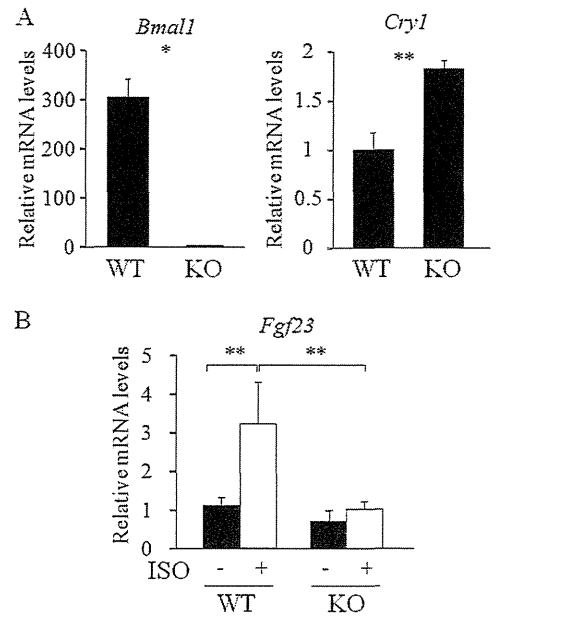

FIGURE 6. **Fgf23 induction by the ISO treatment in the femur was impaired in *Bmal1*-deficient mice.** *A*, the expression of *Bmal1* and *Cry1* was determined by real-time RT-PCR in the femur collected from WT mice and *Bmal1*-deficient mice at ZT16 ($n = 3$–5). *B*, WT mice and *Bmal1*-deficient mice were fed a control diet for 2 weeks from 8 weeks of age, and ISO was injected intraperitoneally at ZT12. Four h after the injection, the expression of *Fgf23* in the femur was analyzed by real-time RT-PCR ($n = 4$–5). Values are expressed as the mean ± S.E. (*error bars*). *, $p < 0.01$; **, $p < 0.05$.

forms of the *Fgf23* gene promoter and found that the luciferase vectors containing CRE1 and CRE2 were responsive to the ISO/IBMX treatment (Fig. 4*C*). To determine the responsible motif(s) for this trans-activation of the *Fgf23* gene promoter, we introduced mutations in CRE1 and/or CRE2 and found that CRE2 was responsible for ISO/IBMX-induced activation of the *Fgf23* gene promoter (Fig. 4*D*).

Overexpression of Cry1 Blunted the Effects of ISO on Fgf23 Induction in UMR-106 Cells—These findings may support the concept that *Fgf23* expression is regulated by sympathetic activity, but it is still unclear as to why *Fgf23* induction by ISO is regulated in a time-dependent manner *in vivo*. To solve this issue, we assessed whether Cry1 was involved in the ISO-induced activation of *Fgf23* expression because Cry1 has been implicated in the suppression of ISO-induced cAMP accumulation in HEK293 cells (36). Indeed, ISO-induced *Fgf23* expression was evident when Cry1 expression was low in the femur (Figs. 1*C* and 3*C*). Based on these results, we tested our hypothesis that Cry1 suppressed ISO-induced *Fgf23* induction by blocking CREB signaling in osteoblastic cells. To test this hypothesis, we overexpressed Cry1 in UMR-106 cells and investigated the effect of ISO on the phosphorylation of CREB. As shown in Fig. 5*A*, the ISO-induced phosphorylation of CREB was impaired in Cry1-overexpressing cells compared with GFP-expressing control cells. In line with this, ISO-induced trans-activation of the *Fgf23* promoter was decreased in cells overexpressing Cry1 (Fig. 5*B*). To further determine the role of the circadian clock network in ISO-induced *Fgf23* induction, we utilized *Bmal1*-deficient mice in which *Cry1* expression was higher than that in WT littermate controls (Fig. 6*A*). The administration of ISO at ZT12 showed a significant increase in *Fgf23* expression in the femur of WT mice, whereas the induction of *Fgf23* was weaker in the femur of *Bmal1*-deficient mice (Fig. 6*B*).

Parathyroid Hormone Induced Fgf23 Expression When Administered at ZT12—Because PTH has been shown to activate the CREB pathway and induce *Fgf23* expression (4, 37), we next tested whether the PTH-induced activation of *Fgf23* was also regulated in a circadian rhythm-dependent manner. To test this hypothesis, we administered PTH(1–34) intraperitoneally to WT mice at ZT0 or ZT12. Four h after the injection, the expression of *Fgf23* was analyzed in the femur. The skeletal expression of *Fgf23* exhibited a significant response to PTH when injected at ZT12, which was associated with a trend toward an increased expression of *Rankl* and a decreased expression of *Sost*, known to be regulated by PTH activation in osteoblastic cells (38), whereas PTH had no effect on *Fgf23* expression when injected at ZT0 (Fig. 7). These results suggest the possibility of the circadian regulation of PTH action with respect to *Fgf23* induction in the skeleton.

Fgf23 Induction by Dietary Phosphate Load Was Not Likely Caused by Sympathetic Activation—Because it is still unclear as to whether circadian *Fgf23* expression is regulated by food intake itself or the influx of phosphate from the diet, we finally tested whether sympathetic activity was involved in *Fgf23* induction by dietary phosphate load. For this purpose, WT mice were fed either a control diet or high phosphate diet for 2 weeks in the presence or absence of PRO. Ingesting the high

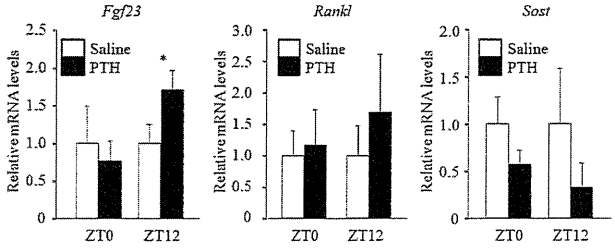

FIGURE 7. **PTH induced skeletal *Fgf23* expression in a circadian fashion.** PTH was intraperitoneally administered in WT mice at ZT0 or ZT12, and samples were collected 4 h after the injection. The expression of *Fgf23*, *Rankl*, and *Sost* in the femur was determined using real-time RT-PCR (n = 3–6). Values are expressed as the mean ± S.E. (*error bars*). *, $p < 0.05$.

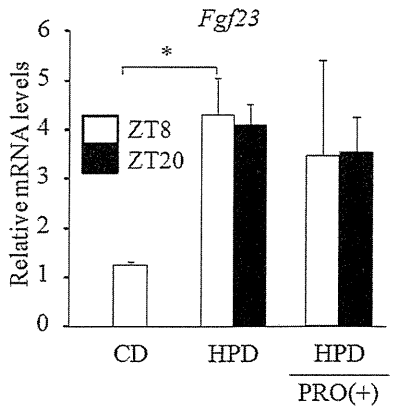

FIGURE 8. **Propranolol did not affect skeletal *Fgf23* expression induced by dietary phosphate load.** WT mice were fed either control diet (*CD*) or high phosphate diet (*HPD*) for 2 weeks from 8 weeks of age in the presence or absence of PRO in the drinking water. The expression of *Fgf23* in the femur was determined using real-time RT-PCR (n = 3–5). Values are expressed as the mean ± S.E. (*error bars*). *, $p < 0.01$.

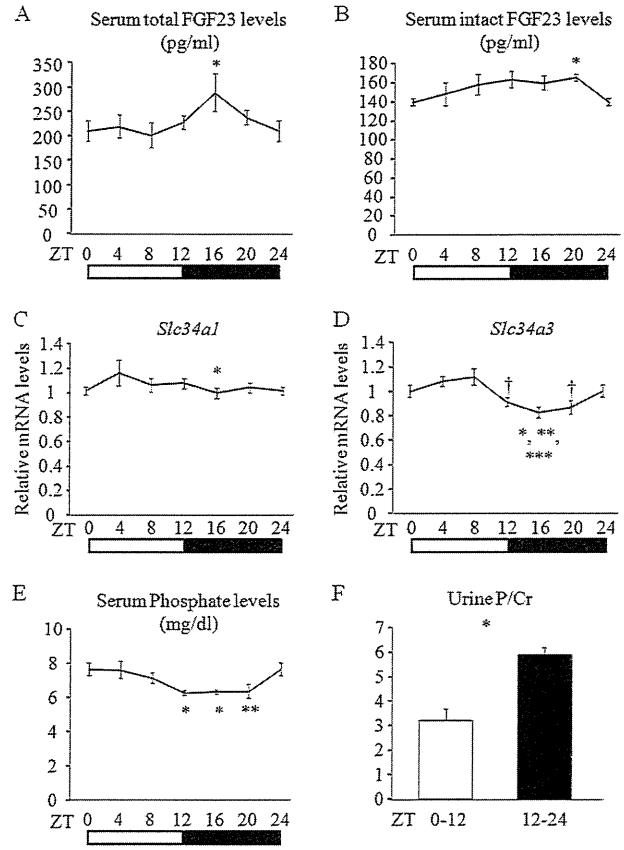

FIGURE 9. **Increase in skeletal *Fgf23* expression during the dark phase was associated with elevated circulating FGF23 levels and enhanced phosphate excretion in the urine.** WT mice were maintained under a light-dark regimen (12-h:12-h cycle) and fed *ad libitum*. Samples were collected every 4 h from ZT0. *A* and *B*, serum concentrations of total (C terminus) FGF23 (n = 6–7, *, $p < 0.05$ *versus* ZT0 and ZT8) (*A*) and intact (full-length) FGF23 (n = 6–7, *, $p < 0.05$ *versus* ZT0) (*B*) were measured. *C* and *D*, the expression of *slc34a1* (n = 6–7, *, $p < 0.05$ *versus* ZT4) (*C*) and *slc34a3* (n = 6–7, *, $p < 0.001$ *versus* ZT8; **, $p < 0.01$ *versus* ZT4; ***, $p < 0.05$ *versus* ZT0; †, $p < 0.05$ *versus* ZT4 and ZT8) (*D*) in the kidney was determined by real-time RT-PCR. *E*, serum concentration of phosphate was measured (n = 7, *, $p < 0.01$ *versus* ZT0; **, $p < 0.05$ *versus* ZT0). *F*, urine was collected either during the light phase (ZT0–12) or dark phase (ZT12–24), and phosphate and creatinine (*Cr*) levels in the urine were measured (n = 9, *, $p < 0.001$). The *white bar* and *black bar* represent the light phase and dark phase, respectively. Values are expressed as the mean ± S.E. (*error bars*).

phosphate diet caused a significant elevation in *Fgf23* expression in the femur (Fig. 8), but the concomitant administration of PRO did not affect the levels of *Fgf23* expression in the femur (Fig. 8), which indicates that the timing of food intake, and not the amount of ingested phosphate, may determine the circadian profiles of skeletal *Fgf23* expression.

The Increase in Skeletal Fgf23 Expression during DP Was Associated with Elevated FGF23 Levels in Serum and Enhanced Phosphate Excretion in the Urine—We finally investigated the association between the increase in skeletal *Fgf23* expression during DP and systemic phosphate metabolism. Consistent with the rhythmic expression pattern of skeletal *Fgf23*, total FGF23 levels in the serum exhibited a circadian expression profile with peak levels at ZT 16 (Fig. 9*A*). Circulating biologically active (intact) FGF23 levels also showed greater levels during DP with the highest at ZT20 compared with ZT0 (Fig. 9*B*). In line with the increased serum FGF23 levels during DP, expression of *Slc34a1* and *Slc34a3* coding for NaP_i-IIa and NaP_i-IIc, respectively, showed decreased expressions during DP (Fig. 9, *C* and *D*, and supplemental Fig. S1), suggesting the enhanced phosphate excretion in the urine during this period. Indeed, serum phosphate concentrations showed a decline during DP associated with enhanced phosphate excretion in the urine (Fig. 9, *E* and *F*). We also analyzed the expression profile of *Cyp27b1* and *Cyp24a1*, other target genes of FGF23 signaling in the kidney, and found that these genes exhibited circadian profiles (Fig. 10). The expression of *Cyp27b1*, which was down-regulated by FGF23 activation, was lower during the DP when FGF23 levels were greater, but the circadian profile of *Cyp24a1*, which was up-regulated by FGF23 activation, did not show any association with that of FGF23, suggesting that circadian profile of genes involved in vitamin D metabolism is mainly regulated by the circadian network independent of circadian FGF23 profiles.

DISCUSSION

In the present study, we demonstrated that skeletal *Fgf23* expression possessed a circadian expression profile. Importantly, the peak in skeletal *Fgf23* expression shifted when mice were maintained under LP-RF regimen, suggesting that timing of food intake is an important determinant for rhythmic expression profile of skeletal *Fgf23*. To investigate the mechanism responsible for generating the rhythmicity in skeletal *Fgf23* expression, we had a hypothesis that sympathetic activity may be the responsible factor linking food intake and skeletal

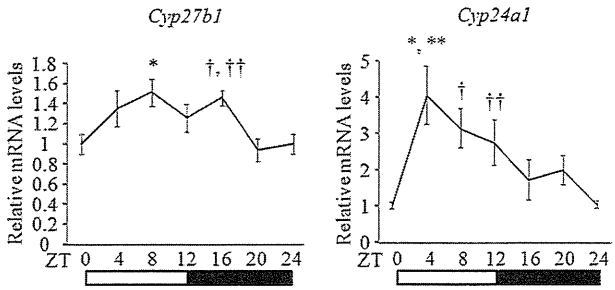

FIGURE 10. **Circadian expression profiles of genes involved in vitamin D metabolism in the kidney.** WT mice were maintained under a light-dark regimen (12-h:12-h cycle) and fed *ad libitum*. Samples were collected every 4 h from ZT0. The expression of *Cyp27b1* ($n = 8–10$, *, $p < 0.01$ *versus* ZT0 and ZT20; †, $p < 0.01$ *versus* ZT20; ††, $p < 0.05$ *versus* ZT0) and *Cyp24a1* ($n = 9–10$, *, $p < 0.001$ *versus* ZT0; **, $p < 0.01$ *versus* ZT16 and ZT20; †, $p < 0.01$ *versus* ZT0; ††, $p < 0.05$ *versus* ZT0) in the kidney was determined by real-time RT-PCR. The *white bar* and *black bar* represent the light phase and dark phase, respectively. Values are expressed as the mean ± S.E. (*error bars*).

Fgf23 expression based on the previous findings that sympathetic activation has been shown to be associated with food intake (28) and display a circadian profile with greater levels during the DP when food intake is active in mice (34). Indeed, we found that the administration of ISO caused an elevation in skeletal *Fgf23* expression in a circadian rhythm-dependent manner. Furthermore, the blockade of sympathetic activity by PRO in mice under LP-RF conditions altered the circadian *Fgf23* expression profile such that the peak expression of *Fgf23* was not observed. Importantly, LP-RF caused a phase shift in sympathetic activity with greater levels during the LF. These results imply that sympathetic activation driven by food intake is a positive regulator for skeletal *Fgf23* expression.

One of the important issues to be addressed is the effect of circadian regulation of skeletal *Fgf23* expression on systemic phosphate metabolism. To address this issue we performed series of analyses and found that circulating both total and biologically active (intact) FGF23 levels were greater during DP. In line with the increase in FGF23 levels during DP, the expression of *slc34a1* and *slc34a3*, known to be down-regulated by FGF23 activation in the kidney, was decreased during this period associated with enhanced phosphate excretion in the urine and decreased phosphate levels in the serum. Because food intake is increased at the beginning of DP in mice, these findings may suggest that the increase in skeletal *Fgf23* expression during DP has an important role in handling the phosphate influx from the diet. It is important to note that the amplitude of circadian profile of intact FGF23 levels is not as obvious as that of total FGF23 levels, suggesting the possibility of the existence of additional mechanism regulating circadian profile of intact FGF23 in the circulation. Because FGF23 protein is known to be cleaved between Arg-179 and Ser-180 (39), it is possible that the post-translational modification or processing of FGF23 protein may create the difference in amplitude between total and intact FGF23 circadian rhythms, although the mechanisms of how FGF23 is cleaved in the circulation are not well defined and still need to be determined. Thus, these lines of evidence may imply that the circadian clock network may function in a coordinated manner involving multiple organs to maintain systemic phosphate homeostasis.

The present findings demonstrate that the timing of food intake regulates the circadian profile of skeletal *Fgf23* expression, but it is still unclear as to whether circadian *Fgf23* expression is regulated by the influx of phosphate from the diet. Because inorganic phosphate has been shown to induce *Fgf23* expression in osteocyte-like IDG-SW3 cells (40), it is possible that the influx of phosphate from the diet may regulate circadian *Fgf23* expression; however, previous *in vivo* studies failed to demonstrate an acute effect of dietary phosphate on FGF23 induction (41, 42), making this concept unlikely to be operative. Despite the lack of an increase in FGF23 levels in response to an acute phosphate load, it has been well established that a chronic phosphate load causes elevations in FGF23 levels (43). Consistent with previous reports, we detected a significant increase in skeletal *Fgf23* expression in mice fed a high phosphate diet, but this increase was not associated with sympathetic activation because the concomitant administration of PRO did not affect *Fgf23* expression. These findings may indicate that the timing of food intake, and not the amount of ingested phosphate, is a predominant determinant for the circadian profiles of skeletal *Fgf23* expression.

The involvement of Cry1 in the regulation of G protein-coupled receptor signaling pathways has been demonstrated previously in a mouse model in which CRE activated luciferase activity in the liver (36). In these mice luciferase activity in the liver was markedly higher at ZT13 than at ZT1, which was associated with increased CREB phosphorylation, and was inhibited when Cry1 was overexpressed (36). The underlying mechanisms described in this study included the suppression of cAMP accumulation by binding of Cry1 to $G_s\alpha$ proteins (36). Based on these previous findings, we investigated whether a similar mechanism was operative in osteoblastic cells and found that overexpression of Cry1 suppressed ISO-induced CREB phosphorylation and trans-activation of the *Fgf23* promoter in osteoblastic UMR-106 cells, which indicated that Cry1 also suppressed ISO-induced *Fgf23* expression in osteoblastic cells. CREB has been shown to bind to the palindromic sequence (TGACGTCA) called CRE with strong affinity and regulate the transcription of target genes. In addition to this canonical CRE, CREB has also been shown to bind to CRE variants albeit with low affinity (44). The sequence of CRE detected in this study is one such variant that is known to mediate CREB signaling (44), and this may be one of the reasons why the induction of luciferase activity by ISO was not intense. Because *in vivo* analysis revealed a significant increase in *Fgf23* expression by the ISO treatment, other CRE motif(s) may be present in other regions and affect the *in vivo* expression of *Fgf23*.

The regulation of *Fgf23* expression in bone has also been implicated in the action of PTH. For example, circulating FGF23 levels were shown to be elevated under conditions in which PTH signaling was continuously active such as chronic kidney disease and Jansen metaphyseal chondrodysplasia caused by a mutation in the *PTH1R* gene, which suggests that PTH is a positive regulator for *Fgf23* expression (37, 45). However, the negative action of PTH on *Fgf23* expression has also been demonstrated in a mouse model in which PTH was intermittently administered (46). Thus, the effect of PTH on *Fgf23* expression is context-specific and controversial (37, 45–47).

Hence, the result showing that the induction of skeletal *Fgf23* by a single injection of PTH was observed in a circadian manner may provide a clue to solve this controversial issue of PTH action on *Fgf23* expression although further studies are needed to precisely determine PTH action on *Fgf23* regulation.

In conclusion, in the present study we have provided evidence that the time of food intake determined the circadian profile of skeletal *Fgf23* expression which involved a systemic activation of sympathetic tone and that sympathetic activation was peripherally regulated by Cry1 expression in the skeleton. Given the paucity of data as to the mechanisms regulating skeletal *Fgf23* expression, these lines of evidence may shed light on new regulatory networks of FGF23 which could be important for understanding the physiology of phosphate metabolism.

Acknowledgments—We thank Yasuhisa Ohata, Jin Nishino, Miwa Yamazaki, and Kanako Tachikawa (Osaka Medical Center and Research Institute for Maternal and Child Health) for critical discussions.

REFERENCES

1. Bergwitz, C., and Jüppner, H. (2011) Phosphate sensing. *Adv. Chronic Kidney Dis.* **18,** 132–144
2. Razzaque, M. S. (2012) The role of Klotho in energy metabolism. *Nat. Rev. Endocrinol.* **8,** 579–587
3. Hubbard, S. R., and Till, J. H. (2000) Protein-tyrosine kinase structure and function. *Annu. Rev. Biochem.* **69,** 373–398
4. Quarles, L. D. (2012) Skeletal secretion of FGF-23 regulates phosphate and vitamin D metabolism. *Nat. Rev. Endocrinol.* **8,** 276–286
5. Martin, A., David, V., and Quarles, L. D. (2012) Regulation and function of the FGF23/Klotho endocrine pathways. *Physiol. Rev.* **92,** 131–155
6. Shimada, T., Kakitani, M., Yamazaki, Y., Hasegawa, H., Takeuchi, Y., Fujita, T., Fukumoto, S., Tomizuka, K., and Yamashita, T. (2004) Targeted ablation of *Fgf23* demonstrates an essential physiological role of FGF23 in phosphate and vitamin D metabolism. *J. Clin. Invest.* **113,** 561–568
7. Urakawa, I., Yamazaki, Y., Shimada, T., Iijima, K., Hasegawa, H., Okawa, K., Fujita, T., Fukumoto, S., and Yamashita, T. (2006) Klotho converts canonical FGF receptor into a specific receptor for FGF23. *Nature* **444,** 770–774
8. Kuro-o, M., Matsumura, Y., Aizawa, H., Kawaguchi, H., Suga, T., Utsugi, T., Ohyama, Y., Kurabayashi, M., Kaname, T., Kume, E., Iwasaki, H., Iida, A., Shiraki-Iida, T., Nishikawa, S., Nagai, R., and Nabeshima, Y. I. (1997) Mutation of the mouse *klotho* gene leads to a syndrome resembling ageing. *Nature* **390,** 45–51
9. Kurosu, H., Ogawa, Y., Miyoshi, M., Yamamoto, M., Nandi, A., Rosenblatt, K. P., Baum, M. G., Schiavi, S., Hu, M. C., Moe, O. W., and Kuro-o, M. (2006) Regulation of fibroblast growth factor-23 signaling by Klotho. *J. Biol. Chem.* **281,** 6120–6123
10. ADHR Consortium. (2000) Autosomal dominant hypophosphataemic rickets is associated with mutations in FGF23. *Nat. Genet.* **26,** 345–348
11. Feng, J. Q., Ward, L. M., Liu, S., Lu, Y., Xie, Y., Yuan, B., Yu, X., Rauch, F., Davis, S. I., Zhang, S., Rios, H., Drezner, M. K., Quarles, L. D., Bonewald, L. F., and White, K. E. (2006) Loss of DMP1 causes rickets and osteomalacia and identifies a role for osteocytes in mineral metabolism. *Nat. Genet.* **38,** 1310–1315
12. Lorenz-Depiereux, B., Schnabel, D., Tiosano, D., Häusler, G., and Strom, T. M. (2010) Loss-of-function *ENPP1* mutations cause both generalized arterial calcification of infancy and autosomal-recessive hypophosphatemic rickets. *Am. J. Hum. Genet.* **86,** 267–272
13. Liu, S., Tang, W., Zhou, J., Stubbs, J. R., Luo, Q., Pi, M., and Quarles, L. D. (2006) Fibroblast growth factor 23 is a counter-regulatory phosphaturic hormone for vitamin D. *J. Am. Soc. Nephrol.* **17,** 1305–1315
14. Shimada, T., Yamazaki, Y., Takahashi, M., Hasegawa, H., Urakawa, I., Oshima, T., Ono, K., Kakitani, M., Tomizuka, K., Fujita, T., Fukumoto, S., and Yamashita, T. (2005) Vitamin D receptor-independent FGF23 actions in regulating phosphate and vitamin D metabolism. *Am. J. Physiol. Renal Physiol.* **289,** F1088–F1095
15. Kolek, O. I., Hines, E. R., Jones, M. D., LeSueur, L. K., Lipko, M. A., Kiela, P. R., Collins, J. F., Haussler, M. R., and Ghishan, F. K. (2005) 1α,25-Dihydroxyvitamin D3 up-regulates FGF23 gene expression in bone: the final link in a renal-gastrointestinal-skeletal axis that controls phosphate transport. *Am. J. Physiol. Gastrointest. Liver Physiol.* **289,** G1036–G1042
16. Nelson, W. (1964) Aspects of circadian periodic changes in phosphorus metabolism in mice. *Am. J. Physiol.* **206,** 589–598
17. Carpenter, T. O., Insogna, K. L., Zhang, J. H., Ellis, B., Nieman, S., Simpson, C., Olear, E., and Gundberg, C. M. (2010) Circulating levels of soluble Klotho and FGF23 in X-linked hypophosphatemia: circadian variance, effects of treatment, and relationship to parathyroid status. *J. Clin. Endocrinol. Metab.* **95,** E352–E357
18. Smith, E. R., Cai, M. M., McMahon, L. P., and Holt, S. G. (2012) Biological variability of plasma intact and C-terminal FGF23 measurements. *J. Clin. Endocrinol. Metab.* **97,** 3357–3365
19. Vollmers, C., Gill, S., DiTacchio, L., Pulivarthy, S. R., Le, H. D., and Panda, S. (2009) Time of feeding and the intrinsic circadian clock drive rhythms in hepatic gene expression. *Proc. Natl. Acad. Sci. U.S.A.* **106,** 21453–21458
20. Green, C. B., Takahashi, J. S., and Bass, J. (2008) The meter of metabolism. *Cell* **134,** 728–742
21. Bass, J., and Takahashi, J. S. (2010) Circadian integration of metabolism and energetics. *Science* **330,** 1349–1354
22. Liu, C., Li, S., Liu, T., Borjigin, J., and Lin, J. D. (2007) Transcriptional coactivator PGC-1α integrates the mammalian clock and energy metabolism. *Nature* **447,** 477–481
23. Damiola, F., Le Minh, N., Preitner, N., Kornmann, B., Fleury-Olela, F., and Schibler, U. (2000) Restricted feeding uncouples circadian oscillators in peripheral tissues from the central pacemaker in the suprachiasmatic nucleus. *Genes Dev.* **14,** 2950–2961
24. Zhang, L., Abraham, D., Lin, S. T., Oster, H., Eichele, G., Fu, Y. H., and Ptáček, L. J. (2012) PKCγ participates in food entrainment by regulating BMAL1. *Proc. Natl. Acad. Sci. U.S.A.* **109,** 20679–20684
25. Fagius, J., and Berne, C. (1994) Increase in muscle nerve sympathetic activity in humans after food intake. *Clin. Sci.* **86,** 159–167
26. Sakaguchi, T., Arase, K., Fisler, J. S., and Bray, G. A. (1988) Effect of starvation and food intake on sympathetic activity. *Am. J. Physiol.* **255,** R284–R288
27. Troisi, R. J., Weiss, S. T., Parker, D. R., Sparrow, D., Young, J. B., and Landsberg, L. (1991) Relation of obesity and diet to sympathetic nervous system activity. *Hypertension* **17,** 669–677
28. Tseng, Y. H., Cypess, A. M., and Kahn, C. R. (2010) Cellular bioenergetics as a target for obesity therapy. *Nat. Rev. Drug Discov.* **9,** 465–482
29. Ralph, M. R., Foster, R. G., Davis, F. C., and Menaker, M. (1990) Transplanted suprachiasmatic nucleus determines circadian period. *Science* **247,** 975–978
30. Kornmann, B., Schaad, O., Bujard, H., Takahashi, J. S., and Schibler, U. (2007) System-driven and oscillator-dependent circadian transcription in mice with a conditionally active liver clock. *PLoS Biol.* **5,** e34
31. Shimba, S., Ogawa, T., Hitosugi, S., Ichihashi, Y., Nakadaira, Y., Kobayashi, M., Tezuka, M., Kosuge, Y., Ishige, K., Ito, Y., Komiyama, K., Okamatsu-Ogura, Y., Kimura, K., and Saito, M. (2011) Deficient of a clock gene, brain and muscle Arnt-like protein-1 (BMAL1), induces dyslipidemia and ectopic fat formation. *PLoS One* **6,** e25231
32. Kondo, H., Nifuji, A., Takeda, S., Ezura, Y., Rittling, S. R., Denhardt, D. T., Nakashima, K., Karsenty, G., and Noda, M. (2005) Unloading induces osteoblastic cell suppression and osteoclastic cell activation to lead to bone loss via sympathetic nervous system. *J. Biol. Chem.* **280,** 30192–30200
33. Takeda, S., Elefteriou, F., Levasseur, R., Liu, X., Zhao, L., Parker, K. L., Armstrong, D., Ducy, P., and Karsenty, G. (2002) Leptin regulates bone formation via the sympathetic nervous system. *Cell* **111,** 305–317
34. Fu, L., Patel, M. S., Bradley, A., Wagner, E. F., and Karsenty, G. (2005) The molecular clock mediates leptin-regulated bone formation. *Cell* **122,** 803–815
35. Elefteriou, F., Ahn, J. D., Takeda, S., Starbuck, M., Yang, X., Liu, X., Kondo,

H., Richards, W. G., Bannon, T. W., Noda, M., Clement, K., Vaisse, C., and Karsenty, G. (2005) Leptin regulation of bone resorption by the sympathetic nervous system and CART. *Nature* **434,** 514–520
36. Zhang, E. E., Liu, Y., Dentin, R., Pongsawakul, P. Y., Liu, A. C., Hirota, T., Nusinow, D. A., Sun, X., Landais, S., Kodama, Y., Brenner, D. A., Montminy, M., and Kay, S. A. (2010) Cryptochrome mediates circadian regulation of cAMP signaling and hepatic gluconeogenesis. *Nat. Med.* **16,** 1152–1156
37. Lavi-Moshayoff, V., Wasserman, G., Meir, T., Silver, J., and Naveh-Many, T. (2010) PTH increases *FGF23* gene expression and mediates the high-*FGF23* levels of experimental kidney failure: a bone parathyroid feedback loop. *Am. J. Physiol. Renal Physiol.* **299,** F882–F889
38. Keller, H., and Kneissel, M. (2005) *SOST* is a target gene for PTH in bone. *Bone* **37,** 148–158
39. Benet-Pagès, A., Lorenz-Depiereux, B., Zischka, H., White, K. E., Econs, M. J., and Strom, T. M. (2004) FGF23 is processed by proprotein convertases but not by PHEX. *Bone* **35,** 455–462
40. Ito, N., Findlay, D. M., Anderson, P. H., Bonewald, L. F., and Atkins, G. J. (2013) Extracellular phosphate modulates the effect of 1α,25-dihydroxy vitamin D3 (1,25D) on osteocyte like cells. *J. Steroid Biochem. Mol. Biol.* **136,** 183–186
41. Larsson, T., Nisbeth, U., Ljunggren, O., Jüppner, H., and Jonsson, K. B. (2003) Circulating concentration of FGF-23 increases as renal function declines in patients with chronic kidney disease, but does not change in response to variation in phosphate intake in healthy volunteers. *Kidney Int.* **64,** 2272–2279
42. Nishida, Y., Taketani, Y., Yamanaka-Okumura, H., Imamura, F., Taniguchi, A., Sato, T., Shuto, E., Nashiki, K., Arai, H., Yamamoto, H., and Takeda, E. (2006) Acute effect of oral phosphate loading on serum fibroblast growth factor 23 levels in healthy men. *Kidney Int.* **70,** 2141–2147
43. Perwad, F., Azam, N., Zhang, M. Y., Yamashita, T., Tenenhouse, H. S., and Portale, A. A. (2005) Dietary and serum phosphorus regulate fibroblast growth factor 23 expression and 1,25-dihydroxyvitamin D metabolism in mice. *Endocrinology* **146,** 5358–5364
44. Smith, B., Fang, H., Pan, Y., Walker, P. R., Famili, A. F., and Sikorska, M. (2007) Evolution of motif variants and positional bias of the cyclic-AMP response element. *BMC Evol. Biol.* **7,** S15
45. Brown, W. W., Jüppner, H., Langman, C. B., Price, H., Farrow, E. G., White, K. E., and McCormick, K. L. (2009) Hypophosphatemia with elevations in serum fibroblast growth factor 23 in a child with Jansen's metaphyseal chondrodysplasia. *J. Clin. Endocrinol. Metab.* **94,** 17–20
46. Samadfam, R., Richard, C., Nguyen-Yamamoto, L., Bolivar, I., and Goltzman, D. (2009) Bone formation regulates circulating concentrations of fibroblast growth factor 23. *Endocrinology* **150,** 4835–4845
47. Saji, F., Shigematsu, T., Sakaguchi, T., Ohya, M., Orita, H., Maeda, Y., Ooura, M., Mima, T., and Negi, S. (2010) Fibroblast growth factor 23 production in bone is directly regulated by 1α,25-dihydroxyvitamin D, but not PTH. *Am. J. Physiol. Renal Physiol.* **299,** F1212–F1217

RESEARCH ARTICLE

AMERICAN JOURNAL OF medical genetics PART A

Overgrowth Syndrome Associated With a Gain-of-Function Mutation of the Natriuretic Peptide Receptor 2 (*NPR2*) Gene

Kohji Miura,[1] Ok-Hwa Kim,[2] Hey Ran Lee,[3] Noriyuki Namba,[1] Toshimi Michigami,[4] Won Joon Yoo,[3] In Ho Choi,[3] Keiichi Ozono,[1] and Tae-Joon Cho[3]*

[1]Department of Pediatrics, Osaka University Graduate School of Medicine, Osaka, Japan

[2]Department of Radiology, Ajou University Hospital, Suwon, Republic of Korea

[3]Division of Pediatric Orthopaedics, Seoul National University Children's Hospital, Seoul, Republic of Korea

[4]Department of Bone and Mineral Research, Osaka Medical Centre and Research Institute for Maternal and Child Health, Osaka, Japan

Manuscript Received: 11 March 2013; Manuscript Accepted: 8 August 2013

The signal pathway of the C-type natriuretic (CNP) and its receptor, natriuretic peptide receptor 2 (NPR2) is involved in the longitudinal growth of long bones. Loss of function mutations at NPR2 cause acromesomelic dysplasia, type Maroteaux, while overproduction of CNP by chromosomal translocation and a gain-of-function mutation at NPR2 have been reported to be responsible for an overgrowth syndrome in three cases and one family, respectively. We identified a four-generation family with an overgrowth syndrome characterized by tall stature, macrodactyly of the great toes, scoliosis, coxa valga and slipped capital femoral epiphysis, similar to those previously reported in association with CNP/NPR2 overactivity. The serum level of amino-terminal proCNP was normal in the proband. A novel missense mutation of *NPR2*, c.1462G>C (p.Ala488Pro) was found to co-segregate with the phenotype in this family. In vitro transfection assay of the mutant NPR2 revealed overactivity of the mutant receptor at baseline as well as with the ligand. This overgrowth syndrome caused by a gain-of-function mutation at *NPR2* should be differentiated from Marfan or related syndromes, and may be categorized along with the overgrowth syndrome caused by overproduction of CNP due to its phenotypical similarity as overgrowth CNP/NPR2 signalopathy.

Key words: tall stature; CNP signal; scoliosis; macrodactyly of the big toe; slipped capital femoral epiphysis

How to Cite this Article:
Miura K, Kim O-H, Lee HR, Namba N, Michigami T, Yoo WJ, Choi IH, Ozono K, Cho T-J. 2014. Overgrowth syndrome associated with a gain-of-function mutation of the natriuretic peptide receptor 2 (NPR2) gene.
Am J Med Genet Part A 164A:156–163.

INTRODUCTION

Natriuretic peptides are a family of hormones/paracrine factors regulating blood volume, blood pressure, ventricular hypertrophy, pulmonary hypertension, fat metabolism, and long bone growth [Potter et al., 2006]. They include atrial natriuretic peptide (ANP; OMIM 600296). CNP binds to a homodimeric transmembrane receptor, natriuretic peptide receptor B/guanylate cylcase B (NPR2; OMIM108961) to increase intracellular level of cyclic guanosine monophosphate (cGMP) [Schulz, 2005]. Several lines of evidence indicate that CNP-NPR2 signaling plays an important role in endochondral ossification [Yasoda et al., 1998; Teixeira et al., 2008]. Inactivation of CNP-NPR2 signaling resulted in dwarfism in both mouse and human. CNP knock-out mice ($Nppc^{-/-}$) or mice with homozygous loss-of-function mutations in *Npr2* result in undergrowth of the skeletal system [Chusho et al., 2001; Tsuji and Kunieda, 2005]. In humans, an autosomal recessive skeletal dysplasia, acromesomelic dysplasia, type Maroteaux (AMDM) characterized by disproportionately mesomelic shortening of the limbs and severe brachydactyly of the hands and feet is caused by homozygous or compound heterozygous loss-of-function mutations in *NPR2* [Bartels et al., 2004]. On the other hand, chronically elevated plasma level of CNP stimulates skeletal

Kohji Miura and Ok-Hwa Kim contributed equally to this work.

Grant sponsor: Ministry for Health, Welfare and Family Affairs Republic of Korea; Grant number: A080588; Grant sponsor: Ministry of Health, Labour and Welfare of Japan; Grant number: KH20Q007a-1.

*Correspondence to:
Tae-Joon Cho, M.D., Division of Pediatric Orthopaedics, Seoul National University Children's Hospital, 101 Daehang-ro Jongno-gu, Seoul 110-744, Republic of Korea.
E-mail: tjcho@snu.ac.kr

Article first published online in Wiley Online Library (wileyonlinelibrary.com): 20 November 2013
DOI 10.1002/ajmg.a.36218

growth in CNP-overproducing transgenic mice [Kake et al., 2009]. In humans, overproduction of CNP due to a chromosomal translocation causes an overgrowth syndrome [Bocciardi et al., 2007; Moncla et al., 2007]. A three-generation Japanese family was recently reported, with an overgrowth syndrome caused by a gain-of-function mutation in *NPR2* [Miura et al., 2012]. We identified and report a four-generation Korean family with similar phenotype and a novel gain-of-function mutation in *NPR2*.

MATERIALS AND METHODS

Clinical Report

This study was approved by the ethics committee at Seoul National University Hospital, and written informed consent was obtained from the proband and family members. An 8-year-old boy visited orthopedic clinic for awkward ambulation and ankle pain on walking. He was a product of normal full term pregnancy with a birth weight 3.2 kg and height 50 cm ($z = -0.04$). His macrodactyly of the big toe was observed since birth, something familiar to his family (Figs. 1 and 2). Developmental milestones were within normal limits. He was recognized as bigger than his age group after the neonatal period. On physical examination at 8 years of age, the height was 145 cm ($z = +3.67$), and weight was 40 kg (>97th centile). He had Marfanoid habitus and arachnodactyly. Neurologic examination was free of abnormal findings. At age 12 years, an unstable slipped capital femoral epiphysis (SCFE) developed on the left hip. Physical examination at this age revealed height 183 cm ($z = +5.19$), weight 71 kg (>97th centile), BMI 21.2 kg/m^2. He showed long and slender fingers and toes, the hallux being remarkably longer than the other toes, ankle valgus deformity, and scoliosis. No anomalies of cardiac valves or the aorta were found on echocardiogram. Blood pressure was within normal limits. No abnormality was observed in ophthalmic and otologic examinations. Hematological, biochemical and endocrinological values including insulin-like growth factor-I (IGF-I) were within normal ranges. However, bone formation and resorption markers were increased—osteocalcin, 118 ng/ml (reference range, 8–50); urinary cross-linked N-telopeptide of type I collagen, 969 BCE/mM creatinine (reference range, 21–83). Bone mineral density of L2-4 as measure by dual energy X-ray absorptiometry (Lunar Prodigy Advance, GE Healthcare, Waukesha, WI) was 0.791g/cm^2 ($z = -0.3$). Considering the tall stature of this patient, this BMD result may suggest presence of more severe osteopenia. Radiological survey of the skeleton showed coxa valga deformity of the femora, slipped capital femoral epiphysis, and lumbar scoliosis (Fig. 3). Arachnodactyly of all fingers and toes; of these, disproportionately long and large great toes were observed. Investigation of the family history revealed a four-generation family with 11 family members including the proband that could be considered to have the same phenotype. Five of 11 affected members were examined. They were characterized by tall stature (exceeded +4 SD compared to age matched control height of Korean population) and markedly long big toes. All of them showed coxa valga deformity with epiphyseal dysplasia of the femoral capital epiphyses and two had SCFE (Fig. 4). Three of them had lumbar scoliosis. The vertebral bodies were tall and showing endplate irregularities and narrowing of the intervertebral disc spaces in four of them. As seen in the clinical phenotype, radiograph of the feet showed extremely elongated metatarsals and assorted phalanges of the great toe symmetrically. The hands of all affected individuals showed arachnodactyly without elongation of specific fingers.

Mutation Analysis

Genomic DNA was extracted from the circulating leukocytes from the proband and family members available (Fig. 1). All the exons of *CNP*, *NPR2*, Natriuretic peptide receptor C (*NPR3*; MIM108962), and fibroblast growth factor receptor 3 (*FGFR3*; MIM134934) were

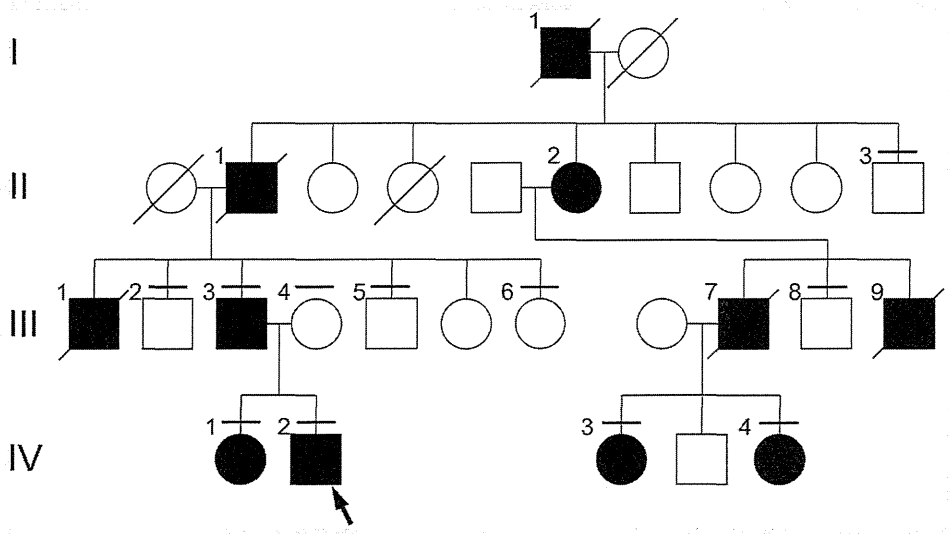

FIG. 1. Pedigree of the family. There are several father-to-son transmissions of the phenotype, revealing autosomal dominant inheritance pattern. Transverse bars above the circles or rectangles denote those who underwent mutation study. An arrow indicates the proband.

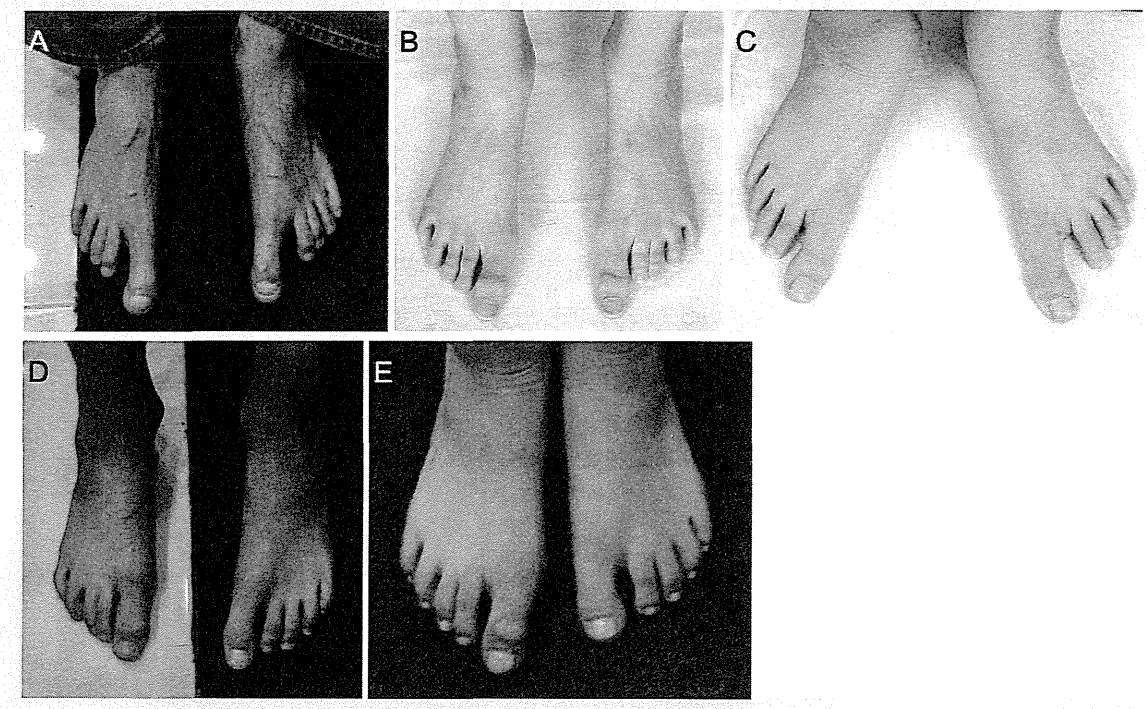

FIG. 2. Photographs of the feet of the affected family members. A: III-3, (B) IV-1, (C) IV-2, (D) IV-3, (E) IV-4. Patients IV-3 and IV-4 show relatively mild macrodactyly of the big toes as compared with the others.

amplified using specific primers [Miura et al., 2012] flanking the intron–exon boundaries according to published human genomic DNA sequences (UCSC genome browser: uc002vsl.1 at chromosome 2, 232498379–232499203; uc003zyd.1 at chromosome 9, 35782406–35799728; uc003jhv.2 at chromosome 5, 32711665–32787252; uc003gds.2 at chromosome 4, 1764337–1780396, respectively). Polymerase chain reaction (PCR) products was sequenced using a Big Dye terminator cycle sequencing kit (version 3.1; Applied Biosystems, Foster City, CA) and an ABI 3130 automated sequencer (Applied Biosystems).

Measurement of Serum Amino-Terminal (NT) proCNP Concentrations

Serum of IV-2 and III-3 were separated and collected, and NT-proCNP was assayed using an enzyme immunoassay (BIOMEDICA, Vienna, Austria) according to the instructions provided. As a control, samples from eight healthy Japanese teenager boys and five women were also measured.

In Vitro Transfection Assay of Mutant NPR2

The pcDNA3.1(+)/hemagglutinin (HA)-tagged human NPR2 wild-type vector (HA-WT) was a gift from Dr. Yoshihiro Ogawa (Tokyo Medical and Dental University, Japan) [Hachiya et al., 2007]. The construct encoding the mutant p.Ala488Pro, pcDNA3.1(+)/HA-human NPR-2 Ala488Pro (HA-Ala488Pro), was generated by PCR-based mutagenesis using HA-WT as the template, and primers containing the nucleotide change. All vector constructs were verified by bidirectional DNA sequencing.

HEK293A cells at confluence were transfected with empty vector containing green fluorescent protein(GFP), HA-WT, and HA-Ala488Pro using the liposomal transfection reagent FuGENE6 (Reagent: DNA = 3 μl: 0.5 μg, Roche, Indianapolis, IN, 12-well plate), according to the manufacturer's instructions. In 48 hr, cell lysate was harvested and immunoblot was performed to compare the expression of transfected genes, using a mouse monoclonal antibody against HA-tag (6E2, 1:1,000; Cell Signaling Technology, Boston, MA) as the primary antibody. As an internal control, β-actin in each sample was detected with a monoclonal anti-β-actin antibody (1:5,000; SIGMA-ALDRICH, Saint Louis, MO).

Transfected cells were serum-starved for 24 hr before the cGMP assay and then incubated at 37°C with 5% CO_2 in DMEM containing 0.5 mM IBMX (3-isobutyl-1-methylxanthine) (Wako, Osaka, Japan) for 10 min. The cells were next treated with vehicle (water) or 1×10^{-7} M CNP-22 (Biochem Life Sciences, New Delhi, India) and incubated for another 10 min. The reaction was terminated with 300 μl of 0.1 M HCl, and the cGMP concentration was measured by a competitive enzyme immunoassay (Cayman Chemical, Ann Arbor, MI). Results are presented as the mean ± SD. Student's *t* test was used for statistical analyses.

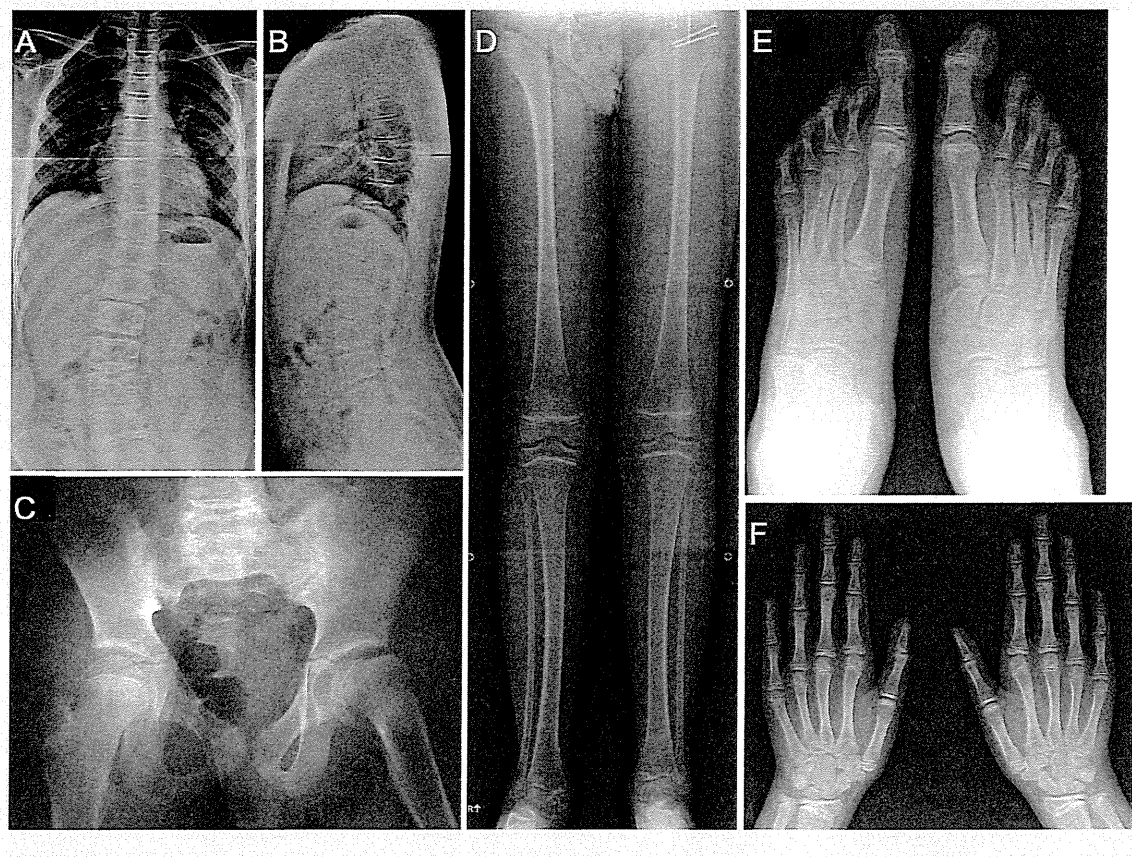

FIG. 3. Skeletal survey of the proband at age 12 years. A,B: Anteroposterior and lateral spine show lumbar scoliosis, slightly tall vertebral bodies with irregular end-plates, and narrowing of the intervertebral disc spaces. C: Pelvis shows coxa valga deformity and slipped femoral capital epiphysis on the left hip. D: Lower extremity demonstrates long and slender long bones with thin cortices. Mild inward bowing of the tibial and fibular diaphysis and ankle valgus deformity are noted. E: Feet show exceedingly long and large metatarsals and phalanges of the great toes symmetrically. F: Hands show overall arachnodactyly without specific digit elongation. Carpal bone age is advanced, measuring approximately 14 years of age.

RESULTS

Identification of a Novel Missense Mutation p.Ala488Pro in *NPR2*

On screening the sequences of exons of *CNP*, *NPR2*, *NPR3*, and *FGFR3* in the proband and family members as depicted on Figure 1, we identified a novel heterozygous sequence variation c. 1462G>C at *NPR2* in those who shared the similar phenotype (III-3, IV-1, IV-2, IV-3, and IV-4), but not in the remaining unaffected family members. The sequence variation eliminates an *Nhe*I cleavage site. PCR product of wild type containing this site (484 bp) would be cut into 95 and 389 bp fragments. Hence, these PCR products from all the patients tested were incubated with *Nhe*I (New England BioLabs, Ipswiich, MA) overnight and run on an agarose gel to confirm the presence of this sequence variation. It showed that this sequence variation perfectly co-segregated with the phenotype in this family. It was predicted to substitute alanine for proline (p. Ala488Pro). This variant was not registered in the dbSNP (build 137) (http://www.ncbi.nlm.nih.gov/projects/SNP/) nor in the NHLBI Exome Sequencing Project (ESP) (http://evs.gs.washington.edu/EVS/). It was not found in 400 alleles from healthy Korean or Japanese controls, either. Amino acid Ala488 is located in a highly conserved region of the juxtamembranous cytoplasmic domain of NPR2 and is conserved across species (Fig. 5). No mutations were found in *CNP*, *NPR3*, or *FGFR3*.

CNP Was Not Overproduced in the Proband

Serum NT-proCNP levels of the proband (IV-2) and his mother were measured 9.68 and 2.65 pmol/L, respectively. Those of eight Japanese teenager boys of age ranging from 12 to 14 years averaged 6.0 ± 3.4 pmol/L (mean ± standard deviation), and of five Japanese female adults of age ranging from 32 to 48 averaged 4.0 ± 0.9 pmol/L (unpublished data).

p.Ala488Pro Is a Gain-of-Function Mutation

To investigate the pathogenic significance of the p.Ala488Pro mutation, an in vitro functional assay was performed. HEK293A

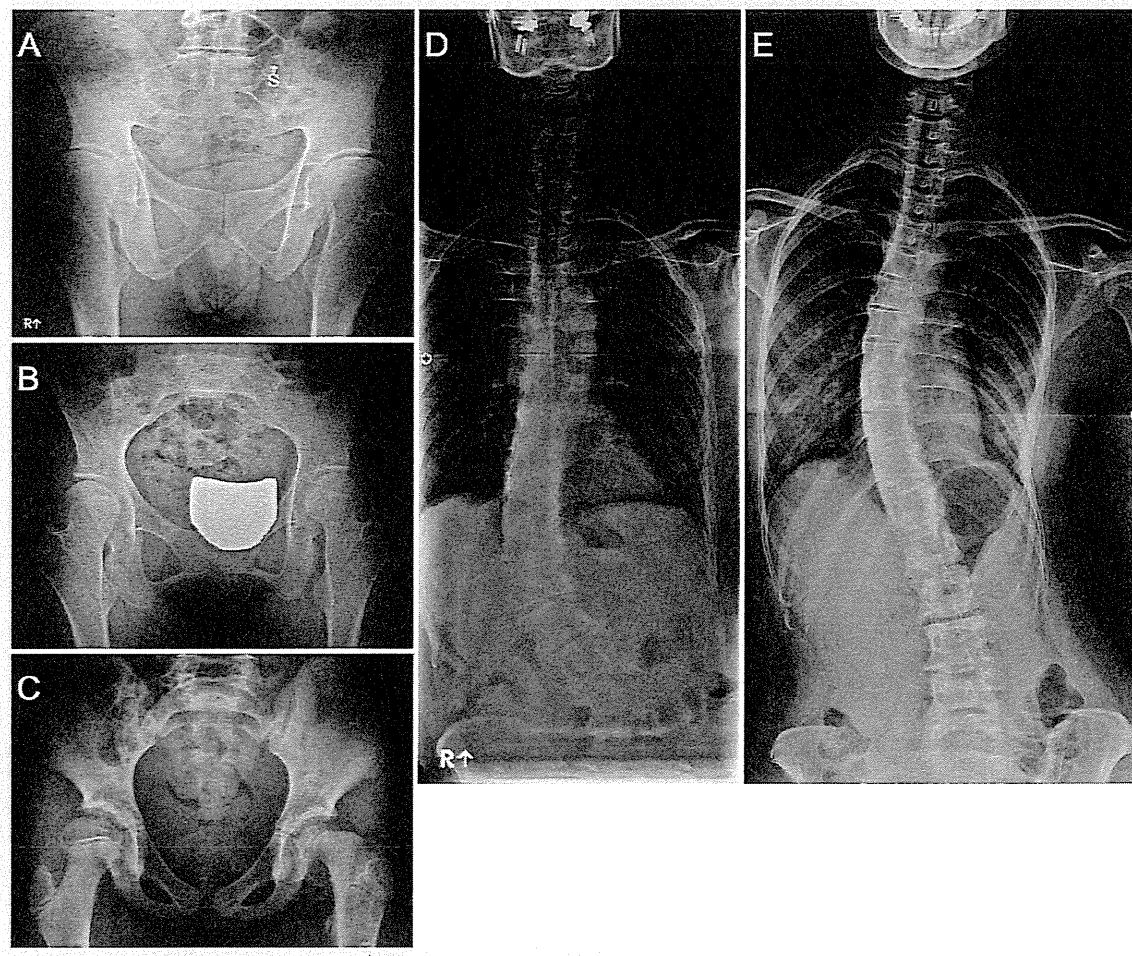

FIG. 4. Radiographs of the pelvis and spine of the other affected family members. Marked coxa valga deformity and residual valgus slipped capital femoral epiphysis are seen in Patients III-3 (A) and IV-1 (B). C: Coxa valga deformity and unstable aggravation of the slipped capital femoral epiphysis at the left hip are seen in Patient IV-3 at age 11 years. D: Patient III-3 and (E) Patient IV-1 show thoracolumbar scoliosis. The vertebral bodies are tall and narrowing of the disc spaces is noted.

cells were transfected with the GFP, HA-WT, and HA-Ala488Pro. The Western blot analysis using anti-HA antibody confirmed that HA-WT and HA-Ala488Pro were expressed at comparable levels, with an approximate molecular size of 120 kDa (Fig. 6A). cGMP production in the cells expressing HA-WT, and HA-Ala488Pro was also examined. cGMP was produced in Ala488Pro-expressing cells, even in the absence of CNP, while no production was observed in HA-WT-expressing cells. Treatment with CNP-22 at a dose of 1×10^{-7} M increased intracellular cGMP levels with concentrations significantly higher in HA-Ala488Pro than in HA-WT-expressing cells (Fig. 6B). These results indicate that p.Ala488Pro is a gain-of-function type mutation.

DISCUSSION

The CNP/NPR2 signal pathway is involved in the longitudinal growth of skeletal system [Yasoda et al., 1998; Chusho et al., 2001; Bartels et al., 2004; Tsuji and Kunieda, 2005; Bocciardi et al., 2007; Moncla et al., 2007; Teixeira et al., 2008; Kake et al., 2009]. Miura et al. [2012] reported a Japanese family with an overgrowth syndrome caused by a gain-of-function mutation at *NPR2*. The current study reports a second family showing a similar phenotype inherited as an autosomal dominant trait. The affected family members harbor a novel gain-of-function mutation at *NPR2*, c.1462G>C (p.Ala488Pro).

The mutation of the current family is located at a topological domain between transmembrane and protein kinase domainsrot[UniProtKB[Internet]], while the previously reported gain-of-function mutation was at the guanylate cyclase domain [Miura et al., 2012]. Although the current mutation does not exist at the guanylate cyclase domain, it must bring conformational change at the 3D structure of guanylate cyclase domain to enhance its enzymatic activity with or without binding the ligand.

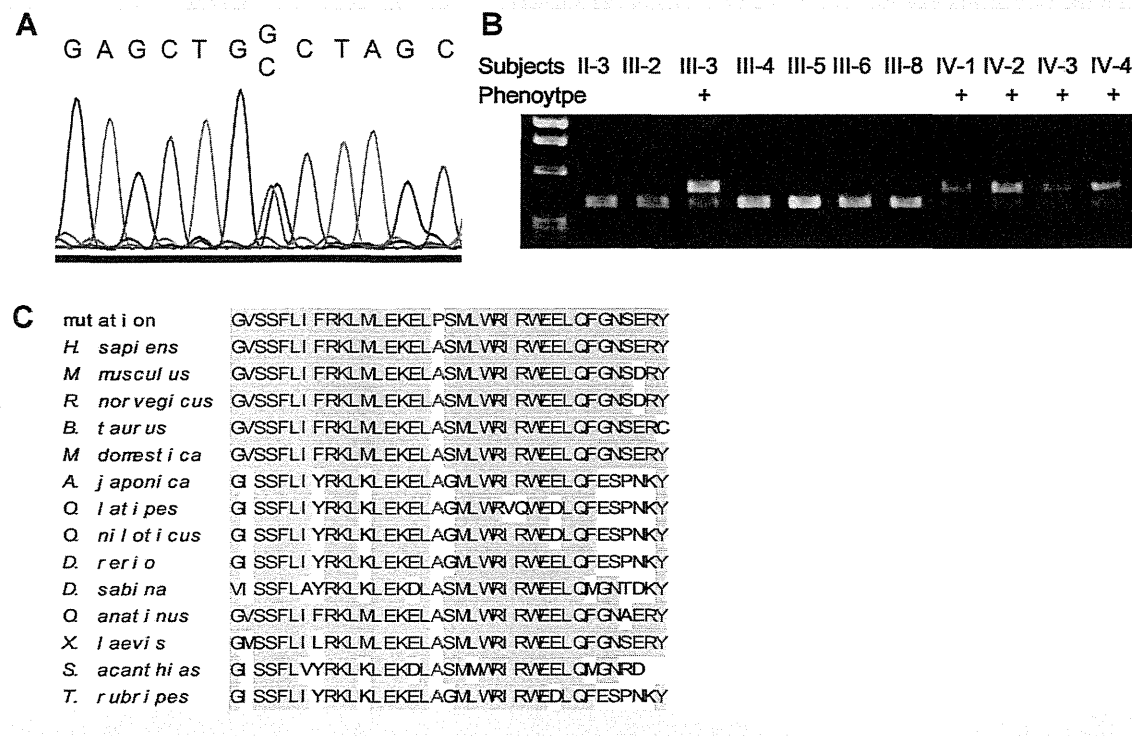

FIG. 5. Identification of the *Npr2* mutation. Sanger sequencing of the *NPR2* revealed a novel G → C missense mutation at nucleotide +1,462 creates a substitution, proline for alanine, at codon 488 in a heterozygous state. Among the subjects tested, this mutation was present in all the patients having the phenotype, and absent in all those who did not (A). This mutation eliminated the cleavage site of *NheI*, producing two bands on gel electrophoresis when treated with *NheI* (B). Amino acid alignment of NPR2 among various species. Alanine at codon 488 is located in a highly conserved cytoplasmic region between the transmembrane and protein kinase domains of NPR2 (C).

NPR2 is an interesting example of phenotypes contrasting between gain-of-function versus loss-of-function mutations at a gene encoding a receptor protein. Homozygous or compound heterozygous loss-of-function mutations of *NPR2* in humans cause a specific skeletal dysplasia, AMDM, characterized by marked short stature as well as short fingers and toes. The overgrowth syndrome by gain-of-function mutation seems to have phenotype opposite to that of AMDM. It is also interesting to note that the increased NPR2 activity did not suppress CNP production, maintaining its serum level within normal limit. The same unsuppressed CNP production was also observed in the previous cases of gain-of-function mutation at *NPR2* [Miura et al., 2012], suggesting lack of feedback loop between the NPR2 activity and CNP production.

This family has noticed 11 affected members by tall stature and long big toes through four generations. Neither macrodactyly of the big toe and ankle valgus deformity nor scoliosis and residual proximal femoral deformity of SCFE interferes with their daily living activities. One of them (IV-3) had even played basketball in a high school varsity team. However, development of unstable SCFE threatened function of the hip joint, and the proband was required to have major hip surgeries. SCFE is a chronic, gradual displacement of the femoral head at the proximal femoral physis. It may remain silent until physeal closure, and end up with residual deformity at the proximal femur as in the Patients III-3 and IV-1 (Fig. 4). However, in some cases, the SCFE could aggravate suddenly, resulting in unstable separation of the femoral head as in Patients IV-2 and IV-4 (Figs. 3 and 4), which is an orthopedic emergency requiring surgical intervention to stabilize the femoral head and to preserve its viability. Hence, once this disease entity is recognized, the patient should have an orthopedic consultation to monitor development and progress of SCFE, which was exclusively harbored by the affected members in this family. It is noteworthy that a residual deformity of silent SCFE showed posterolateral displacement of the femoral head (Fig. 4), a rare subtype of SCFE [Loder et al., 2006]. Scoliosis did not require any intervention in these affected family members. Macrodactyly of the big toes were not complained of in shoe fitting or cosmesis in the proband and affected family members.

The characteristic clinical and radiological findings make it a specific, discernible clinical disease entity, which can be differentiated from Marfan or other related syndromes. However, it is very similar to a phenotype caused by chromosomal translocation of 2q37 and subsequent CNP overproduction [Bocciardi et al., 2007; Moncla et al., 2007]. Hence, CNP overproduction and its receptor gene gain-of-function mutation may be categorized into a disease entity, that is, overgrowth CNP/NPR2 signalopathy, which should be included in differential diagnosis of the overgrowth syndrome.

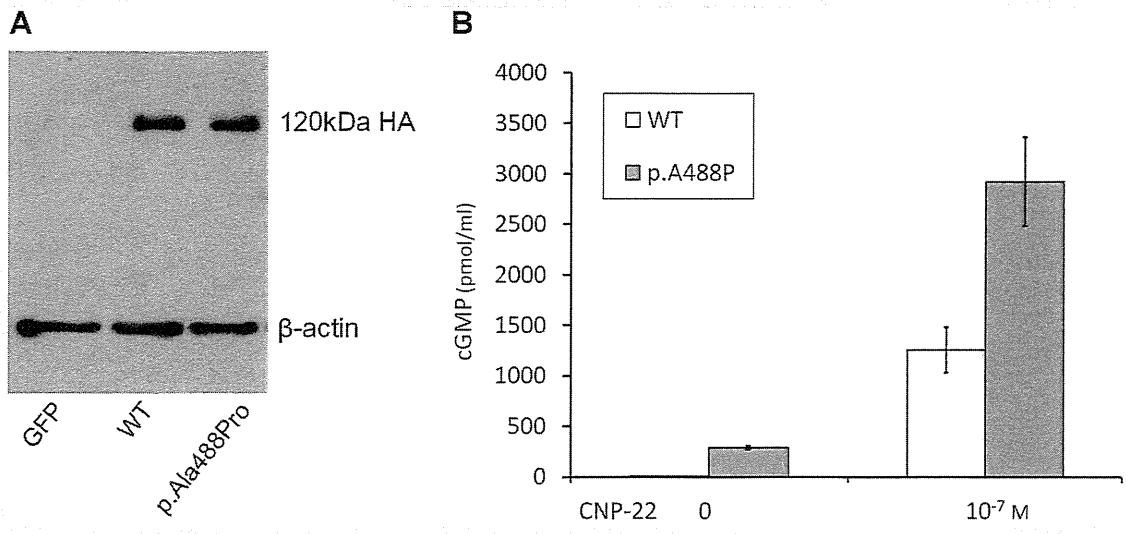

FIG. 6. NPR2 mutation of p.Ala488Pro is a gain-of-function mutation. A: Western blot analysis confirmed the comparable expression of HA-WT (WT) and HA-Ala488Pro. As an internal control, β-actin in each sample was detected with anti-β-actin antibody. B: Increased cGMP production in the HEK293A cells transfected with the p.Ala488Pro mutant compared to that in wild-type cells (WT). Forty-eight hours after the transfection, the cells were serum-starved for 24 hr, and then treated with the indicated concentrations of CNP-22 for 10 min, before cGMP production was assayed. Results are presented as the mean ± SD (N = 3, $^*P < 0.05$).

In summary, we report on a family with an overgrowth syndrome inherited as autosomal dominant trait, which is caused by a gain-of-function mutation at *NPR2*. This is a distinct clinical entity that can be differentiated from other overgrowth syndromes by its clinical and radiological manifestations. Recognition of this specific disease entity will lead to targeted molecular study for confirmation, and will alert the clinician for potentially serious complication such as unstable SCFE.

ACKNOWLEDGMENTS

This study was supported in part by a grant from Ministry for Health, Welfare and Family Affairs, Republic of Korea (A080588) and in part by Grants-in-aid from the Ministry of Health, Labour and Welfare of Japan (KH20Q007a-1).

REFERENCES

Bartels CF, Bukulmez H, Padayatti P, Rhee DK, van Ravenswaaij-Arts C, Pauli RM, Mundlos S, Chitayat D, Shih LY, Al-Gazali LI, Kant S, Cole T, Morton J, Cormier-Daire V, Faivre L, Lees M, Kirk J, Mortier GR, Leroy J, Zabel B, Kim CA, Crow Y, Braverman NE, van den Akker F, Warman ML. 2004. Mutations in the transmembrane natriuretic peptide receptor NPR-B impair skeletal growth and cause acromesomelic dysplasia, type Maroteaux. Am J Hum Genet 75:27–34.

Bocciardi R, Giorda R, Buttgereit J, Gimelli S, Divizia MT, Beri S, Garofalo S, Tavella S, Lerone M, Zuffardi O, Bader M, Ravazzolo R, Gimelli G. 2007. Overexpression of the C-type natriuretic peptide (CNP) is associated with overgrowth and bone anomalies in an individual with balanced t(2;7) translocation. Hum Mutat 28:724–731.

Chusho H, Tamura N, Ogawa Y, Yasoda A, Suda M, Miyazawa T, Nakamura K, Nakao K, Kurihara T, Komatsu Y, Itoh H, Tanaka K, Saito Y, Katsuki M. 2001. Dwarfism and early death in mice lacking C-type natriuretic peptide. Proc Natl Acad Sci USA 98:4016–4021.

Hachiya R, Ohashi Y, Kamei Y, Suganami T, Mochizuki H, Mitsui N, Saitoh M, Sakuragi M, Nishimura G, Ohashi H, Hasegawa T, Ogawa Y. 2007. Intact kinase homology domain of natriuretic peptide receptor-B is essential for skeletal development. J Clin Endocrinol Metab 92:4009–4014.

Kake T, Kitamura H, Adachi Y, Yoshioka T, Watanabe T, Matsushita H, Fujii T, Kondo E, Tachibe T, Kawase Y, Jishage K, Yasoda A, Mukoyama M, Nakao K. 2009. Chronically elevated plasma C-type natriuretic peptide level stimulates skeletal growth in transgenic mice. Am J Physiol Endocrinol Metab 297:E1339–E1348.

Loder RT, O'Donnell PW, Didelot WP, Kayes KJ. 2006. Valgus slipped capital femoral epiphysis. J Pediatr Orthop 26:594–600.

Miura K, Namba N, Fujiwara M, Ohata Y, Ishida H, Kitaoka T, Kubota T, Hirai H, Higuchi C, Tsumaki N, Yoshikawa H, Sakai N, Michigami T, Ozono K. 2012. An overgrowth disorder associated with excessive production of cGMP due to a gain-of-function mutation of the natriuretic peptide receptor 2 gene. PLoS ONE 7:e42180.

Moncla A, Missirian C, Cacciagli P, Balzamo E, Legeai-Mallet L, Jouve JL, Chabrol B, Le Merrer M, Plessis G, Villard L, Philip N. 2007. A cluster of translocation breakpoints in 2q37 is associated with overexpression of NPPC in patients with a similar overgrowth phenotype. Hum Mutat 28:1183–1188.

Potter LR, Abbey-Hosch S, Dickey DM. 2006. Natriuretic peptides, their receptors, and cyclic guanosine monophosphate-dependent signaling functions. Endocr Rev 27:47–72.

Schulz S. 2005. C-type natriuretic peptide and guanylyl cyclase B receptor. Peptides 26:1024–1034.

Teixeira CC, Agoston H, Beier F. 2008. Nitric oxide, C-type natriuretic peptide and cGMP as regulators of endochondral ossification. Dev Biol 319:171–178.

Tsuji T, Kunieda T. 2005. A loss-of-function mutation in natriuretic peptide receptor 2 (Npr2) gene is responsible for disproportionate dwarfism in cn/cn mouse. J Biol Chem 280:14288–14292.

UniProtKB[Internet]. UniProt Consortium (EMBL-EBI, PIR, and SIB) [2002]. P20594(ANPRB_HUMAN) [updated January 9, 2013 Version 151, Cited January 12, 2013]. Available from http://www.uniprot.org/uniprot/P20594

Yasoda A, Ogawa Y, Suda M, Tamura N, Mori K, Sakuma Y, Chusho H, Shiota K, Tanaka K, Nakao K. 1998. Natriuretic peptide regulation of endochondral ossification. Evidence for possible roles of the C-type natriuretic peptide/guanylyl cyclase-B pathway. J Biol Chem 273: 11695–11700.

Pediatr Radiol
DOI 10.1007/s00247-013-2805-z

CASE REPORT

Benign prenatal hypophosphatasia: a treatable disease not to be missed

Masaki Matsushita · Hiroshi Kitoh · Toshimi Michigami · Kanako Tachikawa · Naoki Ishiguro

Received: 21 March 2013 /Revised: 30 May 2013 /Accepted: 15 September 2013

Abstract Prenatal bowing of the long bones is often associated with severe bone dysplasias. We report a child who presented marked bowing of the long bones at birth but showed a relatively benign postnatal course with spontaneous improvement of bowing. The fetal imaging showed normal skeletal mineralization and normal chest and abdominal circumferences despite the limb bowing and shortening. Decreased serum alkaline phosphatase activity and elevated urine phosphoethanolamine was biochemically evident, and compound heterozygous mutations in the tissue-nonspecific alkaline phosphatase (TNSALP) gene were identified, which confirmed the diagnosis of a benign form of prenatal hypophosphatasia. Benign prenatal hypophosphatasia should be considered in the differential diagnosis of congenital bowing of the long bones.

Keywords Benign prenatal hypophosphatasia · Congenital bowing of the long bones · Tissue-nonspecific alkaline phosphatase

Introduction

Prenatal bowing of the long bones occurs in a number of severe bone dysplasias, including osteogenesis imperfecta, campomelic dysplasia, thanatophoric dysplasia and hypophosphatasia. Hypophosphatasia is a rare inherited disorder caused by deactivating mutations within the gene that encodes the tissue nonspecific isoenzyme of alkaline phosphatase (TNSALP). Inorganic pyrophosphate (PPi), a TNSALP substrate and inhibitor of mineralization, accumulates extracellularly, causing rickets or osteomalacia [1]. Traditionally, hypophosphatasia has been classified as being in prenatal, infantile, childhood and adult forms. Those with dental manifestations but no apparent skeletal disease have been called odontohypophosphatasia [2]. The prenatal or infantile forms are often lethal but enzyme-replacement therapy could improve these life-threatening hypophosphatasias [3]. In 1999, Pauli et al. [4] reported four patients who showed intrauterine deformity but had a benign postnatal course. These patients were diagnosed with benign prenatal hypophosphatasia or "Bent but not broken" hypophosphatasia. More than 200 different defects have been identified in TNSALP [5] and these can be autosomal recessive or autosomal dominant inheritance, which helps to explain the extreme range of severity of the disease. Here we describe a boy who presented prenatal bowing of the long bones suggestive of a severe dysplasia but showed favorable postnatal development. Molecular and biochemical analyses confirmed the diagnosis of the sixth form of hypophosphatasia, a benign prenatal hypophosphatasia.

Case report

The boy was the second child of non-consanguineous healthy parents (Table 1). Screening US in the second trimester was thought to show femoral shortness and bowing, thus the mother was referred to our hospital for further assessment. The femoral lengths at 28 weeks and 36 weeks of gestation were 28.1 mm (−8 SD) and 49 mm (−5.8 SD), respectively. But there was no evidence of abnormalities in chest size, abdominal circumference and bone mineralization.

The infant was delivered at 37 weeks of gestation with birth weight of 2,580 g (−1 SD), length of 41.5 cm (−3.5 SD) and head circumference of 32.5 cm (−1 SD). Apgar scores were 8 and 9 at 1 and 5 min, respectively. Shortening and bowing of

None of the authors received financial support for this study.

M. Matsushita · H. Kitoh (✉) · N. Ishiguro
Department of Orthopaedic Surgery,
Nagoya University Graduate School of Medicine,
65 Tsurumai, Showa-ku, Nagoya,
Aichi 466-8550, Japan
e-mail: hkitoh@med.nagoya-u.ac.jp

T. Michigami · K. Tachikawa
Department of Bone and Mineral Research, Osaka Medical Center and Research Institute for Maternal and Child Health, Osaka, Japan

Published online: 22 October 2013

Table 1 Patients' summaries

	Original case	Second case
Prenatal ultrasound	Femoral shortness and bowing	Femoral shortness
Condition at birth		
Gestational age (weeks)	37	38
Length (cm)	41.5 (−3.5SD)	43.7 (−2.5SD)
Weight (g)	2,580 (−1SD)	3,020 (0SD)
Head circumference (cm)	32.5 (−1SD)	33.7 (−0.5SD)
Radiographs at neonatal period		
Rickets	–	–
Bowing	Femurs, tibias, fibulas, humeris	Femurs, radius, ulnas
Short femurs	+	+
Bowdler spur	Bilateral fibulae	–
Extremity skin dimples	+	+
Other clinical concerns	Bilateral clubfeet	–
Delayed developing tooth	Not mentioned	+
Tentative diagnosis	Kyphomelic dysplasia	Caffey disease
Age hypophosphatasia diagnosed (years)	4	1
Biochemical data at diagnosis of hypophosphatasia		
Serum ALP IU/L	139	254
Urinary PEA μmol/day	1,417.4	900.8
TNSALP mutation	p.F327L, c.1559delT	p.R30X, p.F327L
Last evaluation		
Age (years)	5	2
Height (SD)	−1.5	−2
Bowing improvement	++	+

HPP Hypophosphatasia, *ALP* Alkaline phosphatase, *PEA* Phosphoethanolamine, *TNSALP* tissue-nonspecific isoenzyme of alkaline phosphatase, *SD* Standard deviation

the upper and lower limbs, skin dimples on the right forearm and the right lower leg, and bilateral clubfeet deformities were recognized neonatally. Initial radiographs taken on the day of birth showed severe symmetrical bowing and shortening of the long tubular bones with mild metaphyseal widening, and normal ossification of the long bones, skull, vertebrae and ribs (Fig. 1a). A tentative diagnosis of atypical kyphomelic dysplasia was made on the basis of shortening and bowing of the long bones with metaphyseal involvement.

Retrospective reviews of additional radiographs clearly demonstrated the presence of characteristic bony spurs in bilateral fibulae, which looked like the Bowdler spur (Fig. 1b). Laboratory tests including normal serum calcium of 5.0 mEq/l and phosphorus of 5.6 mg/dl, decreased alkaline phosphatase (ALP) of 139 IU/L, and elevated levels of urine phosphoethanolamine (PEA) of 1,417 micro-mol/mg (upper limit of normal is 44 micro-mol/mg) were suggestive of a diagnosis of hypophosphatasia. Genomic DNA was extracted from peripheral blood leukocytes and sequencing analysis confirmed the compound heterozygous mutations (c.979T>C; p.F327L and c.1559delT) in the TNSALP gene.

Physical evaluations at the age of 5 years demonstrated no evidence of limb bowing. The lineal growth was normal with the child's height of 102.9 cm (−1.5 SD). Bowing of the long bones spontaneously improved and fibular spurs disappeared, although the skin dimples still remained (Fig. 2a, b).

Discussion

The differential diagnosis of long bone bowing in utero includes severe disorders that have very poor outcomes and early lethality such as prenatal hypophosphatasia, osteogenesis imperfecta, thanatophoric dysplasia, achondrogenesis and campomelic dysplasia [6]. Despite the severity of long bone bowing, the radiographic evidence of normal bone ossification, normal chest size and normal scapular configuration could differentiate our case from these severe diseases. The Bowdler spur, a bony spur emanating from the midshaft of the fibula toward a subjacent skin dimple, is considered a specific radiographic indicator of hypophosphatasia [7]. Assay of serum ALP activity, and quantification of two natural substrates of TNSALP that accumulate

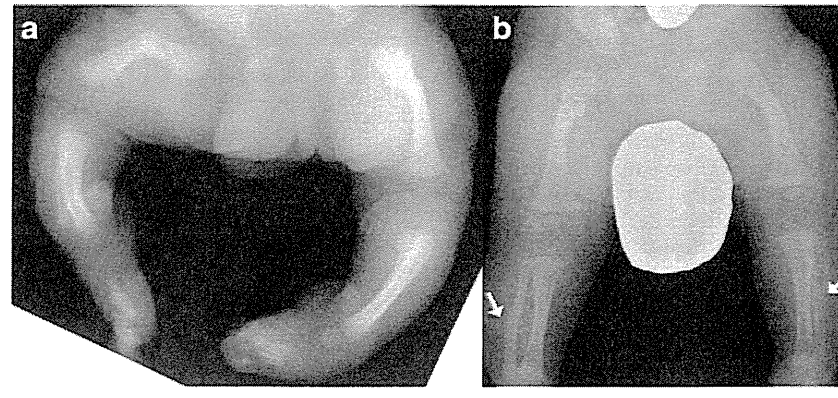

Fig. 1 Anteroposterior radiographs of the lower limbs. **a** A neonatal film shows severe symmetrical bowing and shortening of the long tubular bones with mild metaphyseal widening. **b** A film at the age of 4 months clearly demonstrates bilateral fibular spur (*arrow*)

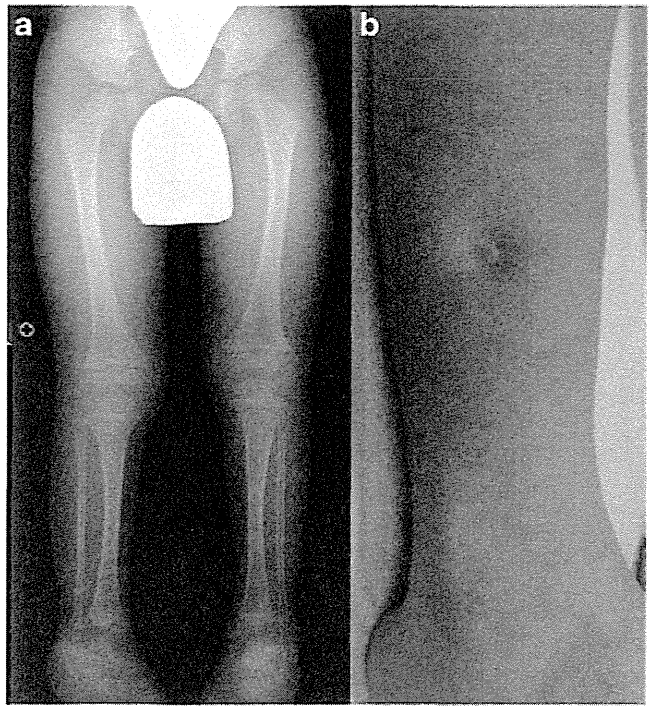

Fig. 2 A 5-year-old boy with prenatal hypophosphatasia. **a** Anteroposterior radiograph of the lower limbs shows improvement of the long bone bowing and disappearance of bilateral fibular spurs. **b** Clinical photo of the right lower limb demonstrates a residual skin dimple

endogenously in hypophosphatasia (pyridoxal 5′-phosphate [PLP] in plasma and PEA in urine) will provide biochemical evidence of hypophosphatasia. Ultimately, definitive diagnosis was made based on molecular testing [8].

Recently, a second boy presented to our institution with benign prenatal hypophosphaatsia (Table 1). The infant was delivered at 38 weeks of gestation with a birth weight of 3,020 g (mean), length of 43.7 cm (−2.5 SD) and head circumference of 33.7 cm (−0.5 SD). Clinical findings at the age of 2 months included shortening and bowing of the thighs and forearms with skin dimples over the site of bilateral forearm angulations. Initial radiographs showed symmetrical bowing and shortening of the femora, radii and ulnae without obvious evidence of fracture or bony spurs (Fig. 3a, b). The humeri, tibiae and fibulae seemed to be normal. The thorax and the vertebral bodies were also normal and the skull was well ossified. He showed normal psychomotor development except for delayed tooth eruption. Laboratory tests revealed low serum ALP of 126 IU/L and elevated levels of urine PEA of 900.8 micro-mol/mg. DNA analysis confirmed the compound heterozygous mutations (c.88C>T; p.R30X and c.979T>C; p.F327L) in the TNSALP gene. Radiographic evaluations at the age of 2.5 years demonstrated persistent but less marked limb shortening and bowing (Fig. 4a, b). The lineal growth was normal with his height of 81 cm (−2 SD).

Mild forms of hypophosphatasia mostly result from heterozygosity for dominant severe alleles or from compound heterozygosity for severe and moderate alleles [8]. Moderate alleles produce significant residual ALP activity, while severe alleles do not usually have enzymatic activity. The F327L mutation has been shown to retain around 70% of enzymatic activity compared with the wild-type protein. On the other hand, c.1559delT mutant identified in the index case, almost completely lost its activity. Michigami et al. [8] reported that patients with F327L mutation in one of the alleles exhibited a relatively mild phenotype despite its prenatal onset, while the c.1559delT mutation was associated with severe forms of hypophosphatasia (prenatal lethal and infantile forms) when not found in patients with the F327L mutation.

Spontaneous improving hypophosphatasia should be added to the list of disorders presenting with prenatal or perinatal bowing of the long bones. We presented several clinical and radiographic characteristics of this specific disease, including congenital bowing and shortening of the long tubular bones that spontaneously improve with time, the Bowdler spur, skin dimples over the site of deformities, tooth abnormalities, and normal ossification of the skull, vertebrae and thorax. Characteristic fetal imaging, including normal bone mineralization, normal chest and abdominal size, and improvement of limb bowing late in the second trimester could lead to the diagnosis of benign prenatal hypophosphatasia, which is a treatable disease.

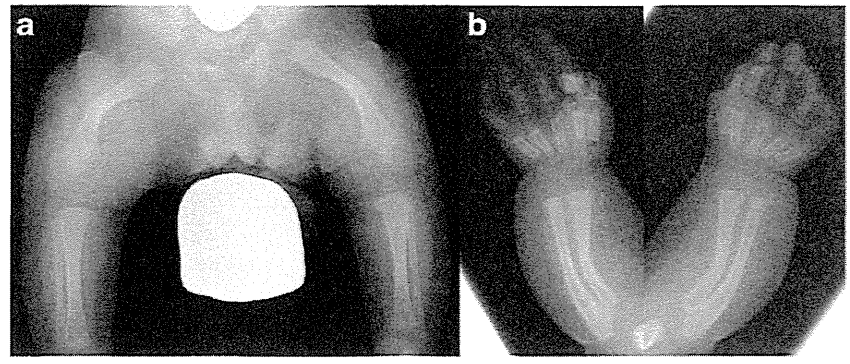

Fig. 3 Anteroposterior radiographs in a 2-month-old boy with prenatal hypophosphatasia. **a** Shortening and bowing of bilateral femora with relatively normal tibiae and fibulae. **b** Marked bowing of the radii and ulnae without evidence of fracture

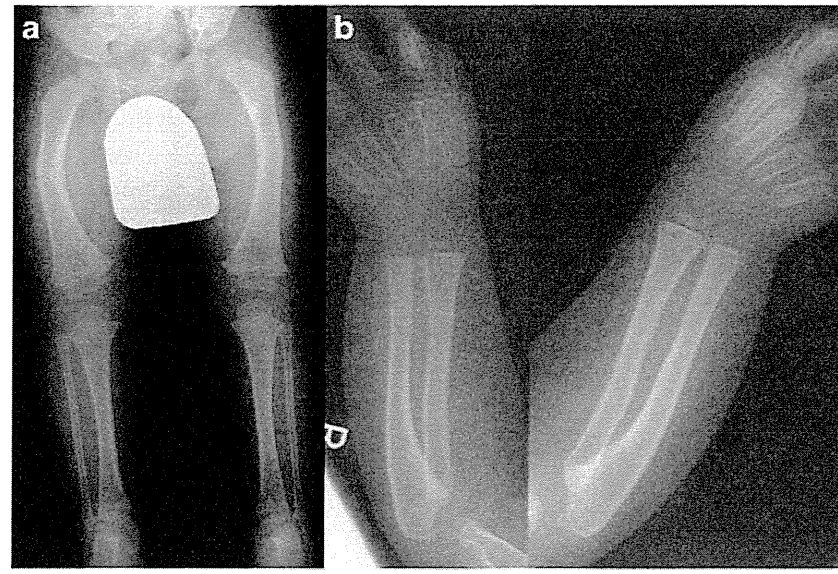

Fig. 4 Anteroposterior radiographs in a 2.5-year-old boy with prenatal hypophosphatasia. **a** Partial improvement of the femoral bowing with cortical thickness at the concave side. **b** Complete healing of the forearm bowing

Conflict of interest The authors declare no conflict of interest.

References

1. Whyte MP (2008) Hypophosphatasia: nature's window on alkaline phosphatase function in humans. In: Bilezikian JP, Raisz LG, Martin TJ (eds) Principles of bone biology, 3rd edn. Academic, San Diego, pp 1573–1598
2. Whyte MP (2012) Hypophosphatasia. In: Glorieux FH, Jueppner H, Pettifor B (eds) Pediatric bone, 2nd edn. Elsevier Academic Press, San Diego, pp 771–794
3. Whyte MP, Greenberg CR, Salman NJ et al (2012) Enzyme-replacement therapy in life-threatening hypophosphatasia. N Engl J Med 366:904–913
4. Pauli RM, Modaff P, Sipes SL et al (1999) Mild hypophosphatasia mimicking severe osteogenesis imperfecta in utero: bent but not broken. Am J Med Genet 86:434–438
5. The Tissue Nonspecific Alkaline Phosphatase Gene Mutation Database. www.sesep.uvsq.fr/03_hypo_mutations.php#mutations. Accessed 9 December 2010
6. Alanay Y, Krakow D, Rimoin DL et al (2007) Angulated femurs and the skeletal dysplasias: experience of the International Skeletal Dysplasia Registry (1988–2006). Am J Med Genet A 143:1159–1168
7. Wenkert D, McAlister WH, Coburn SP et al (2011) Hypophosphatasia: nonlethal disease despite skeletal presentation in utero (17 new cases and literature review). J Bone Miner Res 26:2389–2398
8. Michigami T, Uchihashi T, Suzuki A et al (2005) Common mutations F310L and T1559del in the tissue-nonspecific alkaline phosphatase gene are related to distinct phenotypes in Japanese patients with hypophosphatasia. Eur J Pediatr 164:277–282